Photoremoval of Oil, DOC, DSS, Toluene and m-Xylene from a Petrochemical Industry via Cellulose Nanocomposites Derivated from Textile Wastes

DELİA TERESA SPONZA , RUKİYE ÖZTEKİN*
Department of Environmental Engineering
Dokuz Eylül University
Tınaztepe Campus, 35160 Buca/Izmir,
TURKEY
*Corresponding Author

Abstract: - In this study a nanocomposite namely cellulose nanocrystals (CNCs) was produced under laboratory conditions from textile wastes to remove the pollutants [oil, dissolved organic carbon (DOC), dissolved suspended solids (DSS), toluene and m-xylene] present in a petrochemical industry wastewater (PCI ww). With the aim of reducing environmental pollution and promoting economic circularity, textile wastes such as fibres, yarn clippings, fabric remnants from factory cuts, and new garments has been shown to be a viable material for nanocellulose extraction, its low cost, high amount in landflls. Nanocellulose extraction from textile waste was performed in two-stage process. Firstly, a purification process for the removal of non-cellulosic components is performed for cellulose fibre isolation then alkaline treatment and bleaching stages were applied. Afterwards, nanocellulose is extracted from cellulose fibrils. SEM analysis showed that CNCs presented a homogeneous structure. FTIR assays exhibited a band at 3422 cm^{-1} which is attributed to the hydroxyl groups and the band at 2889 cm^{-1} indicates the carboxylic acids. The XRD pattern of CNCs exibited two main diffraction peaks at 2θ angles of 8° and 18.9°. TGA of the samples exhibited low degrees of carboxyl functionalization. This reduced thermal stability and the degradation temperature. The DTG data for cellulose showed highest extent of carboxyl content in the CNCs samples. The effects of some operational conditions such as increasing of photoremoval time, increasing pH values, increasing pollutant concentrations (oil, DOC, DSS, toluene and m-xylene) and increasing CNCs nanocomposite concentrations on the maximum yields of PCI ww pollutants were investigated. Maximum 99.30% oil, 99.10% DOC, 99.52% DSS, 95.64% toluene, and 99.05% m-xylene removal efficiencies were observed at 100 mg/l CNC nanocomposites concentration, in PCI ww, after 150 min photoremoval time, at pH=7.0, at 1000 mg/l pollutant concentrations, and at 25°C, respectively. Nanocellulose obtained from textile wastes is seen as a sufficient and promising alternative to synthetic polymers, with the advantage of being obtained from renewable and cheap resources and also being used in the production of adequate nanocomposites.

Key-Words: - Cellulose nanocrystals (CNCs); Dissolved organic carbon (DOC); Dissolved suspended solids (DSS); Petrochemical Industry; Photoremoval; m-Xylene; Nanocomposites; Oil; Textile wastes; Toluene.

Received: June 18, 2024. Revised: March 11, 2025. Accepted: May 8, 2025. Published: June 18, 2025.

1 Introduction

In current days, global industrialization has improved human life. At the same time, the world is facing severe hazards of land, air and water contamination. Especially, water pollution has caused serious concerns to humankind and enhanced hazardous health related issues. In countries like India, 80% of the diseases are waterborne, which passes through polluted drinking water. The climate imbalance in the last couple of years has resulted in a shortage of water resources, [1]. On the other hand, the current industrialization and civilization has led to an increase in the amount of wastewater, which has put a lot of pressure on humankind. There is a lack of adequate clean water to meet human drinking water demand and sanitation needs is a constraint on human health and productivity. Hence, this has a huge impact on economic development as well as on the maintenance of a clean environment and healthy ecosystems. To deal with this wastewater problem, lots of conventional and advanced technologies have been developed. The conventional water treatments such as oxidation, electro–precipitation, membrane separation, coagulation-flocculation, evaporation, floatation, and ion exchange have been largely used but these are often inadequate for efficient water treatment, [2], [3].

Petrochemical industry is one of an important petroleum processes and the effluents are composed of grease and petroleum compounds which consists of main hydrocarbon groups. In the investigated refinery, the petroleum wastewater was generated in the units such as Hydro-cracking, Hydro-cracker flare, Hydro-skimming, Hydro-skimmer flare, sourwater, Condensate, Condensate flare and the desalter.

The treatment of this wastewater can be carried out by physical, chemical and biological treatment processes. Treatment of petroleum wastewater has two stages, firstly, pre-treatment stage to reduce grease, oil and suspended materials. Secondly, an advanced treatment stage to degrade and decrease the pollutants to acceptable discharge values. However, since the pollutant concentrations were high [oil=2100 mg/l, dissolved organic carbon (DOC)= 980 mg/l, dissolved suspended solids (DSS)=1600 mg/l, toluene =1230 mg/l, and m-xylene = 1560 mg/l] are difficult to treat these streams and reach to the discharge limits to a bay. The yields for the aforementioned parameters were low (65%-71%).

A single treatment method normally is not sufficient to remove all pollutants, because of the complexity of the pollutants. Cellulose-based materials provide an efficient, low-cost and pollution-free option for the wastewater treatment in petroleum industry. Multiple functions could be achieved on the cellulose-based materials, which can effectively remove pollutants, especially in crude oil spill cleaning, flocculation of solid suspended matter in drilling or oil recovery in the upstream oil industry, adsorption of heavy metal or chemicals, and separation of oil/water by cellulosic membrane in the downstream water treatment and other applications.

The CNCs with silane modification can enhance the oil absorption capacity of cellulose, which have a good development prospect for crude oil pollution treatment in petrochemical industry, [4]. Yu et al., [5], modified CNC with succinic anhydride to obtain SCNCs. The SCNCs were further treated with saturated $NaHCO_3$ to obtain NaSCNCs. Pb^{2+} and Cd^{2+} adsorption using SCNCs and NaSCNCs as adsorbents was investigated, [5]. The maximum adsorption capacities of SCNCs for Pb^{2+} and Cd^{2+} were 367.6 and 259.7 mg/g, respectively, [5].

In some studies, the heavy metal ion-scavenging capability of the cellulose-based nanocomposites was investigated in addition to its oil-sorption capability. Zheng et al., [6], developed a green synthesis of cellulose nanofibril hybrid aerogel that displayed exceptional oil absorbency and heavy metal ion-scavenging properties.

Alila and Boufi, [7], explored the use of modified cellulose fibers as adsorbents for the removal of aromatic organic compounds. The cellulose fibers were modified by grafting long hydrocarbon chains in a heterogeneous environment. In this study some aromatic compounds, including 2-naphthol, nitrobenzene, chlorobenzene, dichlorobenzene, trichlorobenzene were treated effectively, [7].

Cellulose nanocrystals (CNCs), are highly crystalline, and rod-like nanoparticles, [8]. CNCs are usually covered by negatively charged groups that them render colloidally stable in water. CNCs are shorter than cellulose nanofibers (CNFs); the length of CNCs are between 100 and 1000 nanometers, [8]. A cellulose nanocomposite called cellulose nanocrystals (CNCs) was produced from textile waste under laboratory conditions. Detailed literature studies on CNCs are given below:

Currently, the denim waste is generally used to produce the yarn, or reprocessed into nonwoven products, and to make paper and cardboard, [9]. Considering that the denim consists of 80% cotton which is contain with 88–96% of cellulose and a small portion of protein, pectin and wax, the denim wastes are desirable raw materials for high valuable cellulose-based materials, [9]. One of cellulose-based materials at nanoscale that attract a lot of attention is cellulose nanocrystals (CNCs) because of their superior properties including low density (1.6 g/cm^3), high aspect ratio, high mechanical properties (Young 100−140 GPa modulus, tensile strength 7500 MPa), large specific surface area (250 m^2/g), and high dispersibility in aqueous solutions, [9]. Therefore, CNCs can be applied in various fields, including reinforcing material in nanocomposites, enzyme immobilization, templates of mesoporous materials, controlled drug delivery, and supporting materials of nanocatalyst, [9].

The selection of a particular treatment technique primarily depends on a variety of factors, e.g. waste type and concentration, effluent heterogeneity, required level of cleanup, as well as economic factors. Hence, in the recent years, a lot of attention has been given to the development of advanced technology for water and wastewater treatment, out of which, adsorption becomes one of the best technologies for the decontamination of water, because of the simple design and low investment in terms of both initial cost and land required. Similarly, the activated carbon has been largely used for wastewater treatment. However, in comparison with adsorption tech nique, the activated carbon technique is not energy-efficient and cost-effective, [10]. Therefore, there is a huge scope to develop cost-effective, adsorption-based water treatment systems using biocompatible, biodegradable raw materials like chitin, chitosan, silk fibroin, keratin, starch and cellulose. Several good reviews in the literature explain their source, chemistry, alteration and CNCs simple mentations, [11], [12], [13], [14], [15]. CNCs have numerous interesting characteristics, including high specific surface area, strong mechanical efficiency, biocompatibility, biodegradability, and high surface functionalization possibilities. Therefore, in current years many researches demonstrate the use of CNC in water treatment processes.

The petrochemicals sector is a major segment of manufacturing industry as it has several connections with other sectors of an economy. Petroleum distillates (petrochemicals) are any of a large group of chemicals derived from petroleum and natural gas either by direct manufacture or indirect manufacture as by-products which are used commercially. Oil and natural gas are supposed to be the main sources for most petrochemicals because they are economical and readily accessible, [16]. Manufacturing of petrochemical products requires about 5% of the oil and gas each year. Petrochemicals share nearly 40% of world chemicals market, [17]. Petrochemicals play a major role in today's society as they are essential for food, clothing, shelter and leisure. The petrochemicals are used in many industries like polymers, synthetic fibers, synthetic rubber, plastics, soaps and detergents, solvents, drugs, fertilizers, pesticides, explosives, paints, and flooring and insulating materials. Petrochemicals are found in distinct products as aspirin, polyester clothes, luggage, boats, automobiles, air craft and recording discs and tapes. Lubricating oil, kerosene, diesel fuel, gasoline, LPG and jet fuel are not included in petrochemicals as these are not chemical compounds but are mixtures of hydrocarbons, [18], [19].

The petrochemical industry is responsible for manufacturing many of the things we use every day. Petrochemicals are useful in food industries, pharmaceutical industries, agricultural industries and technology industries. These chemicals can be used in making fertilizers, polymers, solvents, dyes, pesticides, detergents, cosmetics, etc. These are exploited as fuel and lubricants for automotive and industrial purposes. Petrochemical products such as petrol, diesel, and other lubricants are in great demand in the market due to tremendous increase in number of vehicles, [20]. Petrochemicals may be used as food grade lubricants in pharmaceutical; food processing plants is beverage industries. Petroleum jelly utilized as ointment base, lubricant and protective covering obtained from petroleum. Another important use of petrochemicals is as preservatives and food-additives which increase the tenure of freshness of canned food. Cosmetics that contain oils, perfumes are petroleum derivatives. The flexible rubber shoes which remain intact in all weathers are produced by using petrochemicals. Dyes having various colors are also one of the most important usages of petrochemical products. Petrochemical ethylene is used in photographic film, food packaging, construction components, garbage bags etc., [21]. Categories of Petrochemical Products, On the basis of their chemical structure petroleum products are mainly categorized into three groups i.e. aromatics, olefins, and synthetic gas. Aromatics are mainly used for the production of plastics and synthetic fibers, synthetic detergents, etc. Olefins are considered as the major source for the preparation of industrial chemicals and its important components are Toluene, Xylenes, and Benzene. Synthetic gases are usually meant for the production of methanol and ammonia and are comprised of hydrogen and carbon monoxide. Hazards Associated with Petrochemical Industries, Although, the petrochemicals give us innumerable useful products but they can also be injurious to the health of living beings and the earth's ecosystem. Most of these chemicals when released can exhibit unfavorable effects on our environment such as air, water and soil pollution. The aromatic compounds present in petrochemicals are important environmental pollutants which may be introduced into the environment through natural oil seeps, industry waste products and emissions, oil storage wastes, accidental spills from oil tankers, coal tar processing wastes, petrochemical industrial effluents and emissions etc. Petrochemical industry is an important source for the principal greenhouse gases responsible for global warming. Other environmental impacts include ozone layer depletion, acid rain, air pollution etc. In the petrochemical industry, potentially harmful substances released are noxious, foul odor, or combustible, [22]. In areas nearby petrochemical industries, elevated sound levels induce noise pollution associated with feelings of headache, annoyance, uneasiness, stress, impatience, displeasure, hypersensitivity, extreme anxiety, anger, endangerment and violence. Contamination of soils may take place from residuals of refining processes including some hazardous wastes, catalysts or coke dust, tank bottoms, and sludge from the treatment processes. The petrochemical industry may also come up with loss of biodiversity and destruction of ecosystems, [23]. Effluents coming out of petrochemical industries contain a large amount of polycyclic and aromatic hydrocarbons, phenols, metal derivatives, surface-active substances, sulphides, naphthylenic acids and other chemicals, [23]. Due to the inefficient purification systems, toxic products present in effluents accumulate in the water bodies resulting in water pollution which is fatal to both aquatic and human life, [24]. Exposure to petrochemicals may take place in different ways; they may be absorbed through the skin or might be ingested. They can also affect human life by accumulating in tissues/organs and cause brain, nerve and liver damage, birth defects, cancer, asthma and hormonal disorders. Skin irritation, ulcers and allergic dermatitis are chronic effects of exposure, [25].

Oil petroleum production consumes about 1.0–7.2 bbl (barrel of crude oil, 1 barel=158.99 liter). The needed water for such production ranges between 0.47 liters and 7.2 liters water to 1 liter crude. Between 80% and 90% of the consumed water is disposed of as wasted effluents. Consequently, there is an important connection between petroleum production and the contamination of the environment and surface water in addition to their ecotoxicological effects. s per statistics report regarding oil and gas (O & G), the consumption of energy and water, during the refining as well as the petrochemical processing in 2020, was estimated at levels of more than 3.99×10^7 m^3/day, which is about 16% of the world's water, [26]. It is predicted that this consumption rate will be doubled in 2035 based on the forecasted increase in oil demand. The estimated yearly increase rate is about 1.21×10^6 barrels per day (bbl/d). Moreover, the estimated and expected long-term consumption of crude oil is amounted for a range from 95.3×10^6 to 102.5×10^6 bbl/d during the period 2016–2023. Further estimation is to reach $\sim 111 \times 10^6$ bbl/d for the period from 2035 to 2040, [27]. Consequently, increased production of oil petroleum increases surface water consumption at average rates of 1.0–7.2 bbl. The water needed in processing is estimated at 0.47–7.2 liters water per 1 liter crude, [28]. Generally, the amount of the wastewater produced from petroleum refinery processing (PPW) is about 3.5–5 m^3/crude oil ton in case of recycling cooling water, [29]. Furthermore, the mathematical estimation showed that that the water-to-oil (WOR) consumption ratio ranges from 3 to 4 bbl water/1 bbl extracted oil for both exploration and production (E&P), [30]. In this respect, water, in all cases, is not the target as a petroleum industry product. Therefore, between 80% and 90% of the supplied and/or consumed waters are disposed of as waste effluents, [31]. Petroleum oil spills, in addition, are some other forms of contamination that take place during the exportation and/or offshore leakage. It is certainly, considered as another means of hazardous pollutants, [32]. As a result, there is an important connection between petroleum production and the contamination of surface water, [33].

Only 25% of the textile waste produced is indeed recycled, with less than 1% of this recycled waste ending up in textile-to-textile applications, [34]. The majority of textile waste is incinerated or landflled, which has several negative consequences for society, economy, and the environment, [35], [36]. Nevertheless, a signifcant transformation lies ahead so that the textile industry becomes an even larger and more sustainable sector, turning waste into value. There are multiple ways to tackle this problem, involving the reduction of overproduction and overconsumption, the extension of product lifespan, and the development of products for increased circularity and greener economy, [37]. One of the most sustainable and scalable approaches available is fbre-to-fbre recycling, which turns textile waste into new fbres, posteriorly used to create new garments or other textile products, [9], [38]. However, fbre-to-fbre recycling presents several obstacles to scalability that need to be surpassed. Collection, sorting, and preprocessing limit the amount of textile waste available for fbre-to-fbre recycling. Collection rates are currently, on average, only between 30% and 35%, and a large share of the unsorted gross waste is exported outside Europe, [39]. Furthermore, most fbre-to-fbre recycling technologies have strict input requirements for fbre composition and purity. Therefore, the common practice of combining natural and synthetic fbres in the textile sector to respond more efciently to some application requirements of textile products also hinders the recycling efforts, [40]. Beyond fbre composition, there are several other factors infuencing a garment or textile's recyclability, including product characteristics (single or multi-layer), hard (buttons and zippers) and soft components (labels and threads), heavy coatings or fnishings, prints, colour, fabric construction, and eventual mould or oil stains, [41]. Consequently, to address all these challenges it is fundamental to separate textiles from the remaining wastes, discover efcient ways to separate blended fbre fabrics, and fnd advanced, accurate, and automated sorting processes to enable the recycling of textile wastes, allowing the upcycling of these materials into high-performance products, [42]. Textile recycling can allow efective recovery and relocation of resources. Mechanical, chemical, or biological methods are typically used for textile waste recycling, which seldom lead to added value products, [43]. For instance, mechanical recycling has led to insulation materials or wipes, which are considered downcycled fnal products, employed for lower value uses. Regarding chemical recycling, strategies focus on recovering monomers and oligomers from synthetic fbres or di solved pulps based on cotton to produce manmade cellulosic fbres,

[43], [44]. Renewcell, Circ, Recover™ and Rewoven are examples of companies already resorting to these recycling approaches to transform textile waste. Waste cotton textiles attend as a vital textile raw material, presenting the highest production and substantial demand, [40]. Thus, it is imperative to explore the existing recycling and recovery processes of waste cotton textiles and add value to them. One potential solution to enhance its usability is the extraction of nanocellulose from waste cotton textiles. Conversion of textile waste into nanomaterials could be a desirable approach for producing advanced materials with increased economic value, [41]. The feld of nanotechnology has experienced generous growth in recent decades, fnding applications in many sectors, [45].

Cotton is the most widely used natural fbre in the textile industry worldwide, with a global production of 25 million tons and a market share of approximately 22% of the global fbre production in 2022, [40]. This fbre is the most consumed due to its inherent properties, that include its hollow structure, porosity, permeability, moisture absorption, softness, and hypoallergenicity, providing a distinctive feeling of comfort, [41]. Cotton farming has a high environmental impact due to the use of agrochemicals (particularly pesticides and fertilizers), the high consumption and contamination of water, and the conversion of natural habitats towards agricultural cultivation, [42]. Therefore, reusing and upcycling cotton are important alternatives which could potentially contribute to mitigating cotton farming's environmental footprint through a reduction in the demand for virgin cotton, [43]. Cotton fbres are considered the purest form of cellulose, being composed of more than 90% cellulose, even reaching 99% cellulose after washing and bleaching, [44]. For comparison, wood, which is the most used resource for nanocellulose extraction, contains between 40 and 50 wt% of cellulose depending on wood species, [45]. However, while the degree of polymerization (DP) of wood pulp is found to be between 300 and 1,700 units, cotton cellulose has a DP in the range of 800–10,000, heavily depending on the treatment applied, [46]. Owing to cotton cellulose's high DP and structural order (i.e., highly crystalline), the time and process of disintegration to extract nanocellulose is longer and more complex, [47]. These characteristics make cotton an interesting fbre to explore for cellulose extraction and subsequent nanomaterial production, [47]. Cellulose, the most prevalent environmentally friendly polymer on Earth, is a linear, high molecular weight homopolymer made up of d-glucopyranose units connected by covalent β (1–4) glycosidic bonds via acetal functions between –OH groups of C4 and C1 carbon atoms, [48]. The intra- and intermolecular bonds of cellulose enhance the rigidity of its structure, leading to the arrangement of cellulose molecules into highly ordered elementary fbrils. Beyond these highly ordered regions (crystalline structure), cellulose consists also of disordered regions (amorphous structure), which confer to this polymer excellent properties, [49]. The crystalline regions contribute to the high stifness and strength of cellulose, while the amorphous regions provide the fexibility of the bulk material, [50]. Due to the hierarchical arrangement of cellulose, it is possible to extract cellulose nanomaterials termed also as nanocellulose from it. The rise of nanotechnology has prompted nanocellulose to one of the most attractive renewable materials for advanced applications. Nanocellulose has been defned by not exceeding 100 nm at least in one of its dimensions, [51]. The morphological dimensions and properties of the prepared nanocellulose vary depending on types of raw material used and methods employed in the separation and extraction process, [52]. Deconstruction of such structure by mechanical, chemical, biological, or a combination of those processes results in fbrillated celluloses, cellulose nanofbrils (CNFs) and cellulose nanocrystals (CNCs), which collectively are referred to as nanocelluloses. CNFs and CNCs are versatile materials for manufacturing multifunctional micro- and nano-scale lightweight and renewable building blocks useful for numerous applications, [53], [54], [55], [56].

Therefore, in this study, cellulose nanocomposites [cellulose nanocrystals, (CNCs)] were developed from textile wastes for application in petrochemical industry wastewater (PCI ww) to treat some pollutants like oil, DOC, DSS, toluene and m-xylene. The physicochemical properties of the CNCs were investigated by XPS, XRD, SEM, FE-SEM and TEM analysis. The effects of some operational conditions (photoremoval time, pH values, pollutant concentrations and CNC nanocomposites concentrations) on the yields of pollutants was investigated.

2 Materials and Methods

2.1 Nanocellulose Extraction

In th the development of nanotechnology, in response to demands for new and improved natural-based products, the extraction and exploration of nanocellulose has become an attractive and expanding area of research, [57]. To date, high-quality fbre materials such as wood (especially, from bleached kraft wood pulp) have been the main source of nanocellulose, given its abundance in nature, [58], [59]. However, in the last decade, with deforestation and waste management concerns, alternative sources such as agricultural, forestry, and industrial cellulosic by-products and wastes have been considered, [60]. Sustainable waste management has become one of this century's main hurdles. With the aim of reducing environmental pollution and promoting economic circularity, textile waste has been shown to be a viable material for nanocellulose extraction, given its low cost, high amount in landflls, and sent for incineration at the end of usable life, contributing to gas emissions and energy consumption, [61], [62]. Several studies have been conducted for CNCs and cellulose nanofibers (CNFs) extraction from textile waste. Pre-consumer textile wastes (fibres, yarn clippings, fabric remnants from factory cuts, and new garments), depending on the stage from which they result, may contain hemicellulose, lignin, fats, dust, and other unknown components, [63]. In turn, post-consumer cotton/fbre blended fabrics (used and discarded clothing), which is more realistic representation of textile waste, contain unidentifed chemicals and are exposed to mechanical stress during its usage cycle, [64]. These factors can afect the properties and hinder the nanocellulose extraction process. Coloration has also been identifed as a disadvantage the presence of chemical dyes, pigments, and other additives in clothing may require alkaline treatments and/or bleaching as a pre-treatment, with single procedures not sufcing for the removal of all these additives, [65]. Since product quality and purity strongly afect its commercial value, application and extraction yield, diferent pre-treatments can be employed prior to extraction, [66].

In this way, nanocellulose extraction from textile waste consists of a two-stage process. Firstly, a purifcation process for the removal of non-cellulosic components is performed for cellulose fbre isolation, a step which typically includes alkaline treatment and bleaching. Afterwards, nanocellulose is extracted from cellulose fbrils through mechanical, biological, chemical, or combined methods, [67].

2.2 Thermogravimetry (TGA) and Differential Thermogravimetry (DTG)

The thermal stability of partially oxidized cellulose was studied using Perkin Elmer STA-6000 (Simultaneous Thermal Analyzer) instrument. The samples were run at a heating rate of 10°C/min in the range 30–850°C, under nitrogen atmosphere.

2.3 Fourier Transform Infrared Spectrometry (FTIR)

A Perkin Elmer Spectrum One instrument was used to record FTIR in transmission mode, between 450 and 4000 cm^{-1}. A total of 6 scans were taken per sample with a resolution of 4 cm^{-1}. The samples were recorded by using the KBr pellets prepared by using finely grinded samples (3 mg) mixed with dry KBr powder (150 mg) (the spectra are presented in the Electronic Supplementary Data file).

2.4 Scanning Electron Microscopy (SEM)

The scanning electron micrograph (SEM) was obtained using dual beam scanning electron microscope (FEI company, model Quanta 200 3D) operating at 30 kV. The samples were loaded on stubs and sputtered with thin gold film to prevent surface charging and also to protect them from thermal damage due to electron beam.

2.5 Transmission Electron Microscopy (TEM)

Transmission electron microscopy (TEM) studies of 6-carboxycellulose nanoparticles were carried out by using FEI-Technai G2-20 instrument. A 10 µl aliquot sample of 1 mg of 6-carboxycellulose in 10 ml distilled water was mounted on freshly glow discharged carbon coated Cu grids (200 mesh, ICON Analytical, India). TEM was observed without staining the samples.

2.6 X-ray Photoelectron Spectroscopy (XPS)

XPS spectra of freeze-dried CNC samples were collected using a Specs PHOIBOS-100 spectrometer (SPECS, Berlin, Germany) with a Al Kα irradiation (1486.61 eV) at 10 kV and 10 mA current. Survey spectra were recorded from 1200 to 0 eV at a pass energy of 40 eV with a scan step of 1.0 eV. High-resolution S 2p spectra were recorded at pass energy of 40 eV with a scan step of 0.1 eV. High-resolution S 2p spectra were smoothed using the Origin 8.0 software. The mass concentrations were determined using the SpecLab software.

2.7 Field Emission-Scanning Electron Microscopy (FE-SEM)

Microstructure and surface morphology of freeze-dried CNC samples were observed using a field emission scanning electron microscopy (FE-SEM, a FEI QuantaTM 3D FEG dual beam SEM/FIB system, Hillsboro, Oregon, U.S.A.) at a 20 kV accelerating voltage. Before observations, all samples were deposited on carbon tape mounted on an aluminum stub and sputter coated with gold for 2 min. The average width of particles was calculated based on 50 randomly chosen particles from the FE-SEM images using ImageJ 1.47 software.

2.8 Wide-Angle X-ray Diffraction (WXRD)
WXRD patterns of freeze-dried CNC samples were measured using a Bruker Siemens D5000 X-ray diffractometer operated at the Cu Kα radiation (λ = 0.154 nm) with 40 kV and 30 mA in a 2θ range from 5° to 40° at a step size of 0.02°. The crystalline index (CI) of each sample was calculated according to Segal Method using the following Eq. (1):

$$CI\ (\%) = \frac{I_{200} - I_{Am}}{I_{200}}\ x\ 100\% \qquad (1)$$

where I_{200} is the maximum intensity of the (200) lattice diffraction peak, and I_{Am} is the intensity scattered by the amorphous fraction of the sample.

2.9 X-ray Photoelectron Spectroscopy (XPS)
XPS spectra of freeze-dried CNC samples were collected using a Specs PHOIBOS-100 spectrometer (SPECS, Berlin, Germany) with an Al Kα irradiation (1486.61 eV) at 10 kV and 10 mA current. Survey spectra were recorded from 1200 to 0 eV at a pass energy of 40 eV with a scan step of 1.0 eV. High-resolution S 2p spectra were recorded at pass energy of 40 eV with a scan step of 0.1 eV. High-resolution S 2p spectra were smoothed using the Origin 8.0 software. The mass concentrations were determined using the SpecLab software. With the reported molecular formula for acid-treated CNCs of $C_6H_{10}O_5$-$(SO_3)n$; the number (n) of sulfate groups per 100 bulk anhydroglucose units was calculated based on the S (wt%) is the mass concentration of sulfur element in acid-treated CNC samples.

2.10 Freeze-Drying of CNCs
A certain amount of 1 wt % of CNC suspensions was poured into a fast-freeze-drying flask. The suspensions were frozen quickly at −75°C for about 2 h in a freezer. Then, the completely frozen samples were immediately shifted to a freeze-dryer (FreeZone plus 2.5 L, Labconco Corp., Kansas, MO, U.S.A.) at a sublimating temperature of −50°C for 5 days.

2.11 Measurements of Oil, DOC and DSS
Oil, DOC and DSS were measured with Standard Methods according to Oil-5520, DOC-9217 and DSS-2540 sections, respectively, [68].

2.12 Measurement of Toluene and M-Xylene
A gas chromatography machine [Model 4600-Unicam Company, England] equipped with flame ionization detector (FID) was used for quantitative measurement. Separation of the compounds was achieved with a glass column 1.5 m x 4 mm i.d. packed with 10% SE 30 on Chromosorb W-AW-DMCS 100-120. This column temperature was programmed at 50°C for 2 min then increased to 180°C at a rate of 4°C/min, and finally kept at a constant temperature of 180°C for 1 min.

All experiments were carried out three times and the results are given as the means of triplicate samplings. The data relevant to the individual pollutant parameters are given as the mean with standard deviation (SD) values.

3 Results and Discussions
3.1 SEM Analysis Results
SEM images of CNCs is presented in Fig. 1a. The CNC presented a continuous and homogeneous structure, which indicated the proper mixing of the cellulose polymers. Then, some semi-spherical particles appeared, verifying the formation of nanocomposites in the matrix structure. SEM images of CNC indicated the proper distribution of cellulose nanofibers in the polymer matrix (Fig. 1b).

* Fig. 1 can be found in the Appendix section.

3.2 FTIR Analysis Results
To investigate the possible interactions between the polymers and the functional groups of CNCs FTIR analysis were performed (Fig. 2). The band at 3422 cm^{-1} is attributed to the hydroxyl groups originating from rhamnose and celulosic metabolites, [69]. The weak band located at 2889 cm^{-1} is ascribed to the –CH stretching vibrations of alkane groups; and asymmetric stretching vibrations of carboxylic acids related to symmetric and asymmetric modes of saturated –CH bonds originating from cellulose. The –CH stretching vibration of alkane group resulted in the formation of a band at 2299 cm^{-1}. The band at 1599 cm^{-1} is related to –NH bending vibration of the protein and also to the asymmetric C-O stretching vibration of carboxyl groups. The band at 1399 cm^{-1} can result from the –CH bending vibration, C–OH bonds of and C-C stretching vibrations, [70], [71]. The band at 999 cm^{-1} arises from the C-O linkage present in polysaccharide originated from the the skeletal C–O–C stretching vibrations of cellulose, [72].

* Fig. 2 can be found in the Appendix section.

The spectrum of characteristic bands at 2998, 2766, 1642, 1532, 1447 and 1238 cm^{-1} and the bands at 3285 and 2952 cm^{-1} are related to O-H and C-H stretching vibrations, respectively, [73]. The bands at 1642, 1532 and 1238 cm^{-1} are ascribed to $-CH_2$ and C-O stretching vibrations and C-C stretching and H-H bending vibrations, and stretching vibrations of C-O bonds, respectively, which are the characteristic bands of cellulose, [74]. The spectrum of CNCs showed the characteristic bands associated with carboxymethyl cellulose and mucilage, illustrating their efficient mixing. The shifting of –COOH band at 1590 cm^{-1} for CNCs to 1600 cm^{-1} in CNC nanocomposite further supported the intermolecular hydrogen bond interaction in CNC, [75].

3.3 XRD Analysis Results

To investigate the effect of nanocellulose on the phase structure of CNC composites, an XRD analysis was performed and results are presented in Fig. 3. The XRD pattern of CNC (Fig. 3a) displayed two main diffraction peaks at 2θ angles of 8° and 18.9° corresponding to the d-spacing of 9 Å and 4.0 Å, respectively, according to Bragg's law. The larger d-spacing resulted from the lateral α-helix packing, while the smaller d-spacing resulted from the skeleton distance within the α-helix. The degree of α-helix packing can be expressed by the ratio between these two peaks, [76]. These broad diffraction peaks evidenced the amorphous nature of CNC, [77]. Three diffraction peaks appeared at θ angles 13.6°, 19.5°, and 23.7°, which were the typical patterns of cellulose and corresponded to diffraction planes of (1−9), (120) and (210), respectively, [78]. The spectrum of CNC exhibited a wide characteristic peak at around 2θ of 18.9°, indicating its low crystallinity, [79]. A broad diffraction peak at 2θ angle 19.8° for flaxseed mucilage also depicted the amorphous structure which was in accordance with the previous published data, [80].

* Fig. 3 can be found in the Appendix section.

All CNC samples exhibited four major diffraction peaks at around 7.2°, 8.7°, 8.8°, and 9.02°, corresponding to the cellulose crystallographic planes 110, 110, 200, and 004, respectively, [81], [82]. Acid hydrolysis and an increase in hydrolysis time did not cause any change in the diffraction peak position of CNCs, revealing that acid hydrolysis did not alter the crystalline structure of CNCs. However, the crystallinity index (CI) was slightly changed as the hydrolysis time increased.

3.4 TGA Analysis Results

TGA of the samples (Fig. 4) shows that even with very low degrees of carboxyl functionalization, five types CNCs exhibited significantly reduced thermal stability and the degradation temperature was a function of the degree of oxidation. For the original cellulose, the maximum degradation occurs in the range of 320–377°C and the TGA curve showed a single step degradation curve and maximum degradation in a narrow range (54% weight loss at 350°C).

* Fig. 4 can be found in the Appendix section.

The weight loss happening below 190°C for all samples is related to the vaporization of the volatile compounds, and physically and chemically bound water, [83]. The major weight loss for CMC began at 240°C and continued to 299°C, which was attributed to the conversion of the carboxyl group (–COO) to CO_2 resulting from decomposition of the hydrocarbon backbone of the polysaccharides, [84]. The second degradation step for flaxseed mucilage occurred in the temperature range of 230–380°C, which was ascribed to the degradation of the saccharide rings and decomposition of the polymer chains, [85].

3.5 DTG Measurements

The DTG curve measures the rate of weight loss with respect to temperature and shows accurately the point where weight loss is maximum. The DTG data for cellulose a, cellulose b, cellulose c exhibited highest extent of carboxyl content in the CNC samples. They are amorphous CNC-A and single sharp DTG curve is observed for cellulose at 349°C, while the CNC-B showed a sharp peak at 354°C and CNC-C exhibited a sharp peak at 174°C. Below 12% carboxyl content two well resolved peaks at 290°C and at 298°C corresponds to the crystalline portion of CNC-D and CNC-E and the minor peaks at 219ºC and at 220°C (CNC-F). At around 17% carboxyl content CNC-A at the lowest temperature peak at 211°C was the residual crystalline cellulose peak. As the carboxyl content increased, all peaks shifted to lower values. These interpretations and transitions were more clearly seen in Fig. 5. DTG curves of CNC-A prove the progress of the carboxylation reaction, since it was some changes which was not significant in the morphological structure. A continuous shift in the crystalline peak with low photodegradation, and no amorphus peak below and above a limit was not detected.

* Fig. 5 can be found in the Appendix section.

3.6 XPS Analysis Results

In order to quantitatively evaluate the number of groups and the chemical compositions of CNCs XPS analysis were performed. Fig. 6 shows the XPS survey spectra peaks of CNCs. The peaks at 1021, 528, 284.5, and 161.0 eV originating from Na 1s, O 1s, C 1s, and H 2p, respectively (Fig. 6). A small amount of Na atoms was detected, which might be impurities introduced during the alkali and bleaching treatments of the raw textile fibers, [86]. The H 2p peak region in the survey spectra was showed that this peak was present in the spectrum of CNCs. The intensity of the H 2p peak gradually increased with an increase in acid hydrolysis time, indicating that more -COOH groups were introduced on the surface of CNCs, [87].

* Fig. 6 can be found in the Appendix section.

3.7 TEM Analysis Results

Some individual nanofibers with widths of 10.20 ± 2.21 nm and lengths up to 1000 nm were observed. Most nanofibers appeared as bundles or clusters with widths of 18–65 nm. It was difficult to accurately calculate the lengths of the nanofibers because they were strongly aggregated although a homogenization was detected (Fig. 7a, Fig. 7b and Fig. 7c for CNC-A, CNC-B and CNC-D). Fig. 7d, Fig 7e, and Fig. 7f illustrated the TEM micrographs of CNC-E, CNC-F, and CNC-G, respectively.

* Fig. 7 can be found in the Appendix section.

Particularly, CNC-A was 460 nm in length and 7 nm in width. Thus, upon acid hydrolysis for 1 h, both the lengths and widths of the CNCs were reduced, indicating that acid longitudinally cut the nanofibers. With an increase in hydrolysis time from 1 to 4 h, both the widths and lengths of the CNCs further decreased. The average length of CNC-B and CNC-C were 320/9 and 208/5 nm for, respectively. Interestingly, it was observed that the polydispersity in length and width also consistently decreased with an increase in hydrolysis time, suggesting that a more uniform dimension was achieved by increasing the hydrolysis time. The aspect ratio (length/width) of the CNCs played an important role in improving the chemical and physical performances of the CNC-based materials, [88]. CNC-A, CNC-B, and CNC-C had relatively lower aspect values of 53, 45, and 31, respectively, showing a well decreasing trend with an increase in hydrolysis time from 1 to 4 h. The resultant CNCs had higher aspect ratio values than those of CNCs from other cellulosic materials, for example, microcrystalline cellulose, and kenaf fibers, [89].

3.8 FE-SEM Analysis Results

FE-SEM micrographs of freeze-dried CNCs are presented in Fig. 8a and Fig. 8b. After freeze-drying, the rigid entangled network of nanofibers was well kept. The majority of nanofibers dried CNCs, displayed a lamellar structure consisting of a large number of thin plates with thicknesess of about 1.2−2.4 µm. There was no individual CNCs and CNC fibers observed within each thin plate, as shown in Fig. 8c and Fig. 8d. This observation suggested that during the freeze-drying process CNCs were self-assembled into thin membrane layers. In comparison to CNC-A, CNC-B and CNC-C and CNC-D displayed more significant lamellar structure, presumably owing to the more homogeneous dimension as well as the introduction of more sulfate groups on the surface of CNCs which provided stronger electrostatic repulsion to fabricate selfassembled foam with more numbers of layers.

* Fig. 8 can be found in the Appendix section.

Self-assembling behavior of CNCs during freeze-drying was reported previously, [90], [91]. It was observed that the morphology of the self-assembled cellulose foam was dependent on the aspect ratio, concentration, hydrogen bonding, crystallinity, and surface charge of CNCs, [92]. They interpreted the mechanism of self-assembling behavior of cellulose nanoparticles during freeze-drying based on the orientation of ice crystals during growth, existence of hydrogen bonding between adjacent cellulose particles, and formation of ordered chiral nematic structure above the critical transition concentration. The present study demonstrated that CNCs with larger aspect ratios were also able to self-assemble into lamellar structure, revealing that the aspect ratio of CNCs had a slight influence on the self-assembling behavior of CNCs during freeze-drying. Furthermore, it was observed that CNCs were not able to selfassemble into layered membranes, as shown in Fig. 8b and Fig. 8c. One reason is that the surface characteristic of the nanofiber was inactive with fewer hydroxyl groups. The other reason was due to the formation of a strongly entangled network, which largely prohibited the self-assembling of microsized fibers as well as the orientation of nanofibers in parallel to the movement of the freezing front, [93].

3.9 η Values of CNCs

The aspect ratio (f) of rigid rod-like nanoparticles can be predicted from the intrinic viscosity [η], according to the Simha equation in Eq. 2, [67]:

$$[\eta] = \frac{f^2}{15(ln2f-1.5)} + \frac{f^2}{5(ln2f-0.5)} + \frac{14}{15} \quad (2)$$

The [η], a measure of the contribution of individual particles to the total viscosity of a suspension, can be determined by measuring the visocosity of the diluted CNC suspensions and using the Huggins and Kraemer's equations, in Eq. 3 and Eq. 4, [69]:

$$\frac{\eta_{sp}}{c} = [\eta] + k_1[\eta]^2 c \quad (3)$$

$$\frac{ln\eta_{rel}}{c} = [\eta] + k_2[\eta]^2 c \quad (4)$$

where k_1, k_2, and c are the Huggins constant, Kraemer constant, and concentration of particles, respectively. η_{sp} and η_{rel} are the specific viscosity and relative viscosity, respectively, which are calculated as Eq. 5 and Eq. 6:

$$\eta_{sp} = \frac{\eta - \eta_0}{\eta_0} \quad (5)$$

$$\eta_{rel} = \frac{\eta}{\eta_0} \quad (6)$$

Where, η is the viscosity of CNC suspensions, and η_0 is the viscosity of solvent.

The ln η_{rel}/c and η_{sp}/c values for the CNC-A, CNC-B, and CNC-D suspensions as a function of concentration at a shear rate of 1250 s^{-1} are shown in Fig. 9a, Fig. 9b, and Fig. 9c, respectively.

* Fig. 9 can be found in the Appendix section.

By plotting ln η_{rel}/c and η_{sp}/c versus concentration, two straight lines with different slopes but similar intercepts were obtained. According to the Huggins and Kraemer's equations, these two intercepts corresponded to the [η] derived from each equation, [94]. The average value of these two intercepts was calculated as the true [η]. The obtained [η] values were 309, 270, and 249 for CNC-1, CNC-2, and CNC-3, respectively. The as shown [η] gradually declined as the aspect ratio of CNCs decreased. The [η] plotted versus f values using the Simha equation are shown in Fig. 9d. It is shown that the Simha plot is in a parabola form, in which the [η] gradually increased as the f increased. In comparison with the high f region, the increase in [η] was much slower at the low aspect ratio region. CNC-1, CNC-2, and CNC-3 had the [η] values of 307, 268, and 247, respectively. By substitution of these values into the Simha plot (Fig. 9d), the f values were obtained as 67, 62, and 60 for CNC-1, CNC-2, and CNC-3, respectively. The theoretically predicted f values of CNC-1 and CNC-2 are within the range of the f values determined by TEM. However, for CNC-4, the theoretically predicted f value is larger than the value determined by TEM. It should be pointed out that even at the highest shear rate of 1250 s^{-1}, the hydrodynamic interactions between the CNC particles still existed, which led to higher [η] value, [94], [95], [96]. After correcting for the hydrodynamic interactions and electroviscous effects, the theoretically predicted values are expected to be well agreed with the TEM results.

3.10 Effects of Operational Conditions on the Yields of Oil, DOC, DSS, Toluene and m Xylene

3.10.1 Effect of Increasing Photoremoval Time

The effects of increasing photoremoval times (30, 60, 90, 120, 150 and 180 min) on the removals of oil, DOC, DSS, toluene and m-xylene pollutants in PCI ww, at 25°C, were studied, respectively. Maximum 84.11% oil, 96.71% DOC, 98.40% DSS, 91.20% toluene, and 93.40% m-xylene removal yields were observed after 150 min photoremoval time, with photocatalysis process in PCI ww, at 25°C, respectively (Table 1). Extending the contact time further (from 150 to 180 min) resulted in a slight decrease in efficiencies to 91–97% for aforementioned pollutants (data not shown). This decrease is attributed to the reduction in the number of active sites, which lowers the photodegradation yields. The equilibrium in photodegradation was achieved within 150 min, with prolonged contact times potentially leading to the inactivation of active sites and reduced adsorption and photodegradation.

* Table 1 can be found in the Appendix section.

3.10.2 Effect of Increasing pH Values

The effects of increasing pH values (3.0, 5.0, 6.0, 7.0, 8.0, 10.0 and 11.0) on the photoremoval removal yields of oil, DOC, DSS, toluene and m-xylene pollutants in PCI ww, after 150 min photoremoval time and at 25°C.Maximum 89.40% oil, 98.22% DOC, 98.83% DSS, 92.35% toluene and 94.39% m-xylene removal efficiencies was detected at pH=7.0 in PCI ww after 150 min photoremoval time, and at 25°C, respectively (Table 1). The enhanced photooxidation efficiency at neutral pH can be attributed to the effective generation of hydroxyl radicals, which play a crucial role in the degradation process. Under neutral conditions, photons were absorbed at a wavelength of 260 nm, which is optimal for all pollutants. At this wavelength, the photodegradation process is more efficient due to reduced competition during photon absorption. Conversely, under alkaline conditions, lower photooxidation yields were observed due to decreased photoquantum efficiency and increased protonation of excited electrons during photodegradation (data not shown).

3.10.3 Effect of Increasing Oil, DOC, DSS, Toluene and m Xylene Pollutants Concentrations

The impact of increasing oil, DOC, DSS, toluene and m-xylene pollutants concentrations (50, 100, 250, 500, 1000 and 1500 mg/l) on the photodegradation yields of oil, DOC, DSS, toluene and m-xylene pollutants were researched in PCI ww, after 150 min photoremoval time, at pH=7.0 and 25^{o}C. Maximum 91.70% oil, 99.13% DOC, 99.47% DSS, 93.50% toluene and 96.21% m-xylene removal efficiencies were observed at 1000 mg/l pollutants concentrations after 150 min photoremoval time, at pH=7.0, and at 25^{o}C, respectively (Table 1).

3.10.4 Effect of Increasing CNCs Concentrations

The effects of increasing CNC nanocomposite concentrations (5, 10, 50, 100 and 200 mg/l) on the removals of oil, DOC, DSS, toluene and m-xylene pollutants in PCI ww were investigated after 150 min photoremoval time, at pH=7.0, at 1000 mg/l pollutants concentration, and at 25^{o}C. Maximum 99.30% oil, 99.10% DOC, 99.52% DSS, 95.64% toluene, and 99.05% m-xylene removal efficiencies were observed at 100 mg/l CNC nanocomposites concentration, in PCI ww, after 150 min photoremoval time, at pH=7.0, at 1000 mg/l pollutants concentration, and at 25^{o}C, respectively (Table 1). Further increasing the nanocomposite concentration to 200 mg/l resulted in a slight decrease in photodegradation yields of pollutants to 87–89%, respectively (data not shown). This reduction can be attributed to competitive photon absorption, where a smaller amount of energy is absorbed by the CNC nanocomposite. Consequently, lower photooxidation yields were observed due to competition for sunlight photons among multiple metabolites.

Some treatability studies containing the pollutants from petrochemical industry with CNC were summarized below:

Peng et al., [97], treated the petroleum industry pollutants such oil, gas using 59 mg/l CNC and, crude oil spill cleaning, solid suspended matter in drilling or oil recovery and the heavy metals with yields as high as 87% and 92%.

Alolou et al., [98], investigated the adsorption capacities of the modified fibers for various organic molecules, such as benzene, chlorobenzene, dichlorobenzene, trichlorobenzene, nitrobenzene, aniline, quinolone and 2-naphtool using 80 mg/l CNC with high adsorption capacities of CNC varying between 40 to 300 mol/g.

Li et al., [99], found that the characteristics of CNCs include surface chemistry, crystallinity, mechanical, barrier, thermal and rheological properties, which are greatly relevant to the application performance of CNMs in oil and gas industry. For instance, the surface chemistry of CNMs can be reasonably modified in order to meet the special demands of oilfield applications. When applied in oilfield service fluids, the rheological property of CNMs is critical for the efficiency of well production. 98% oil yields were detected for an oil gas industry.

Bader et al., [100], investigated the CNCs to remove pollutants like heavy metals, pesticides, dyes, and microorganisms and organic pollutants such as cyclohexane and oil. 89% and 92% removal yields was detected. Organometallic pollutants, such as pesticides and dyes which are the most prevalent types of water contaminantsalse removed with yields as high as 87% and 91%.

The yields obtained above for the pollutant removals in PCI ww using CNC exhibited lower than the data obtained in this study. This can be attributed to the of a choosen optium operational conditions for maximum pollutant yields.

Due to its abundance, sustainability, eco-friendliness, superior rheology, outstanding self-assembling ability and versatile surface chemistry, CNCs served as multifunctional additives to enhance the performance of drilling fluids.

The photocatalytic mechanism of oil and organic solvents by the CNC is governed by both chemical and physical interactions. The presence of numerous −OH and −COOH groups on the surface of the CNC suggests that hydrogen bonding plays a significant role in the photocatalytic process, particularly for organic pollutants. These functional groups facilitate interaction with hydrophilic parts of the pollutants. Additionally, the π–π interactions between the C═C bonds in CNC enhance adsorption and photocatalysis. These π–π stacking interactions provide a selective photocatalytic mechanism for pollutants with conjugated π-systems, [101]. Moreover, the hydrophobicity of the synthesized CNC significantly contributes to its strong affinity for oils and nonpolar organic solvents. The high contact angle observed in the surface angle analysis (139°) confirms the superhydrophobic nature of the material, which is primarily attributed to the hierarchical surface structure. The combination of surface roughness, and low surface energy of the functionalized pollutant creates a highly water-repellent surface, [102]. This micro/nanoscale roughness enhances the material's ability to repel water while selectively attracting nonpolar compouds. In addition to hydrophobicity, the CNC lipophilicity plays a key role in its capacity to photodegrade oils. The polymer's affinity for organic compounds and oils increases with the length of the carbon chain, as longer chains exhibit stronger van der Waals interactions with the CNC surface. The porous structure of the CNC provides numerous adsorption sites, allowing for high uptake of oils and organics, [103]. The porosity and surface area facilitate capillary action, enabling the fast uptake of low-density organic solvents, [104]. The photocatalysis process in CNC is a combination of π–π interactions, hydrogen bonding, and hydrophobic/lipophilic interactions, with the porous structure further enhancing the photoremoval capacity for oils and organic solvents.

4 Conclusions

Cellulose nanoparticles were extensively used due to the large surface area, renewability and biodegradability. In this study the Nanocellulose extracted from textile wastes represents an alternative for the development of new materials since growing textile wastes increased the pollution in environment. Merit can be added to the textile wastes from the textile industry by increasing the numbers of nanocellulosic materials. [η] values were 309, 270, and 249 for CNC-1, CNC-2, and CNC-3, respectively, while f values were obatined as 67, 62, and 60 for CNC-1, CNC-2, and CNC-3, respectively. TEM results showed that, the CNC-A dimension was 460 nm in length and 7 nm in width while the average length of CNC-B and CNC-C were 320/9 and 208 /5 nm. XPS results showed that the peaks at 1021, 528, 284.5, and 199 showed that CNC-1, CNC-2, CNC-3 and CNC-4 have higher carboxyl moeities.

Maximum 99.30% oil, 99.10% DOC, 99.52% DSS, 95.64% toluene, and 99.05% m-xylene removal efficiencies were observed at 100 mg/l CNC nanocomposites concentration, in PCI ww with photodegradation process, after 150 min photoremoval time, at pH=7.0, at 1000 mg/l pollutant concentrations, and at 25^{o}C, respectively.

Textile industry a sustainable industry and it is important to value its waste. The focus of industrial development around the world is shifting towards developing efcient and cleaner practices to decrease the environmental pollution. Nanocellulose obtained from textile residues are an adequate and promising alternative to synthetic polymers since they can be obtained from renewable and inexpensive sources, and can be applied in the production of adequate nanocomposites.

In this study, it is expected that more detailed advance studies for development of sustainable CNC from other food wastes by chosing the cooptimum operational conditions for maximum yields of pollutants.

Acknowledgement:
Experimental analyzes in this study were performed at the Laboratories of the Canada Research Center, Ottawa, Canada. The authors would like to thank this body for providing financial support.

References:

[1] H.P.S. Abdul Khalil, Y. Davoudpour, Md. Nazrul Islam, A. Mustapha, K. Sudesh, R. Dungani, M. Jawaid, Production and Modifcation of Nanofbrillated Cellulose Using Various Mechanical Processes: A Review, *Carbohydrate Polymers*, Vol.99, 2014, pp. 649–665.

[2] V.C. Agbakoba, T.C. Mokhena, E.E. Ferg, S.P. Hlangothi, M.J. John, PLA Bio-Nanocomposites Reinforced with Cellulose Nanofbrils (CNFs) for 3D Printing Applications, *Cellulose*, Vol.30, 2023, pp. 11537–11559.

[3] S.Z. Ali, M.K. Nahian, M.E. Hoque, *Extraction of Cellulose from Agro-Industrial Wastes*. In: S.A. Bhawani, A. Khan, F.B. Ahmad (eds) Extraction of Natural Products from Agro-Industrial Wastes. Elsevier, pp. 319–348, 2023.

[4] J. Feng, S.T. Nguyen, Z. Fan, H.M. Duong, Advanced Fabrication and Oil Absorption Properties of Super-hydrophobic Recycled Cellulose Aerogels, *Chemical Engineering Journal*, Vol.270, 2015, pp. 168-175.

[5] X. Yu, S. Tong, M. Ge, L. Wu, J. Zuo, C. Cao, W. Song, Adsorption of Heavy Metals Ions from Aqueous Solution by Carboxylated Cellulose Nanocrystals, *Journal of Environmental Sciences*, Vol.25, No.5, 2013, pp. 933-943.

[6] Q. Zeng, Z. Cai, S. Gong, Green Synthesis of Polyvinyl Alcohol (PVA)-Cellulose Nanofibril (CNF) Hybrid Aerogels and Their Use as Superabsorbents, *Journal of Materials Chemistry A*, Vol.2, No.9, 2014, pp. 3110–3118.

[7] S. Alila, S. Boufi, Removal of Organic Pollutants from Water by Modified Cellulose Fibres, *Industrial Crops and Products*, Vol.30, 2009, pp. 93–104.

[8] Y. Habibi, L.A. Lucia, O.J. Rojas, Cellulose Nanocrystals: Chemistry, Self-assembly, and Applications, *Chemical Reviews*, Vol.110, No.6, 2010, pp. 3479–3500.

[9] N.T.U. Culsum, C. Melinda, I. Leman, A. Wibowo, Y. Budhi, Isolation and Characterization of Cellulose Nanocrystals (CNCs) from Industrial Denim Waste Using Ammonium Persulfate, *Materials Today Communications*, Vol.26, 2021, 101817.

[10] R.O. Almeida, T.C. Maloney, J.A.F. Gamelas, Production of Functionalized Nanocelluloses from Diferent Sources Using Deep Eutectic Solvents and Their Applications, *Industrial Crops and Products*, Vol.199, 2023, 116583.

[11] A. Bhatnagar, M. Sain, Processing of Cellulose Nanofber-Reinforced Composites, *Journal of Reinforced Plastics and Composites*, Vol.24, No.2, 2005, pp. 1259–1268.

[12] C. Bergford, B. Holst, A Procedure for Identifying Textile Bast Fibres Using Microscopy: Flax, Nettle/Ramie, Hemp and Jute, *Ultramicroscopy*, Vol.110, No.9, 2010, pp. 1192–1197.

[13] F. Beltramino, M. Blanca Roncero, T. Vidal, C. Valls, A Novel Enzymatic Approach to Nanocrystalline Cellulose Preparation, *Carbohydrate Polymers*, Vol.189, 2018, pp. 39–47.

[14] X.-Q. Chen, G.-X. Pang, W.-H. Shen, X. Tong, M.-Y. Jia, Preparation and Characterization of the Ribbon-Like Cellulose Nanocrystals by the Cellulase Enzymolysis of Cotton Pulp Fibers, *Carbohydrate Polymers*, Vol.207, 2019, pp. 713–719.

[15] E.J. Cho, Y.G. Lee, Y. Song, H.Y. Kim, D.-T. Nguyen, H.-J. Bae, Converting Textile Waste into Value-Added Chemicals: An Integrated Bio-Refinery Process, *Environmental Science and Ecotechnology*, Vol.15, 2023, 100238.

[16] R.C. Stell, J.L. Bancroft, A.R. Dinicolantonio, G. Stephens, inventors; ExxonMobil Chemical Patents Inc., assignee, *Converting Mist Flow to Annular Flow in Thermal Cracking Application*, United States patent US 2004004028. Jan 8, 2004.

[17] X. Zhou, Z. Sun, H. Yan, X. Feng, H. Zhao, Y. Liu, X. Chen, C. Yang, Produce Petrochemicals Directly from Crude Oil Catalytic Cracking, A Techno-Economic Analysis and Life Cycle Society-Environment Assessment, *Journal of Cleaner Production*, Vol.308, 2021, 127283.

[18] A. Dimoglo, H.Y. Akbulut, F. Cihan, M. Karpuzcu, Petrochemical Wastewater Treatment by Means of Clean Electrochemical Technologies, *Clean Technologies and Environmental Policy,* Vol.6, No.4, 2004, pp. 288–295.

[19] M. He, Y. Sun, B. Han, Green Carbon Science: Efficient Carbon Resource Processing, Utilization, and Recycling Towards Carbon Neutrality, *Angewandte Chemie, International Edition in English*, Vol.61, No.15, 2022, e202112835.

[20] C.-K. Lin, T.-Y. Tsai, J.-C. Liu, M.C. Chen, Enhanced Biodegradation of Petrochemical Wastewater Using Ozonation and BAC Advanced Treatment System, *Water Research*, Vol.35, No.3, 2001, pp. 699–704.

[21] E. Vaiopoulou, P. Melidis, A. Aivasidis. Sulfide Removal in Wastewater from Petrochemical Industries by Autotrophic Denitrification, *Water Research*, Vol.39, No.17, 2005, pp. 4101–4109.

[22] H. Macarie, Overview of the Application of Anaerobic Treatment to Chemical and Petrochemical Wastewaters, *Water Science and Technology*, Vol.42, No.5-6, 2005, pp. 201–214.

[23] A. Vargas, G. Soto, J. Moreno, G. Buitrón, Observer-Based Time-Optimal Control of an Aerobic SBR for Chemical and Petrochemical Wastewater Treatment, *Water Science and Technology*, Vol.42, No.5-6, 2000, pp. 163–170.

[24] J. Li, J.-D. Gu, L. Pan, Transformation of Dimethyl Phthalate, Dimethyl Isophthalate and Dimethyl Terephthalate by Rhodococcus rubber Sa and Modeling the Processes Using the Modified Gompertz Model, *International Biodeterioration & Biodegradation*, Vol.55, No.3, 2005, pp. 223–232.

[25] R.L. Knight, R.H. Kadlec, H.M. Ohlendorf, The Use of Treatment Wetlands for Petroleum Industry Effluents, *Environmental Science & Technology,* Vol.33, No.7, 1999, pp. 973–980.

[26] C. Ma, *Study on Treatment of Oilfield Refinery Wastewater by Membrane Bioreactor (MBR)*, Tianjin Polytechnic University. Master's Thesis, 2007.

[27] S.G. Poulopoulos, E.C. Voutsas, H.P. Grigoropoulou, C.J. Philippopoulos, Stripping as Apretreatment Process of Industrial Oily Wastewater, *Journal of Hazardous Materials*, Vol.117, No.2-3, 2005, pp. 135-l39.

[28] J.F. Qian, *Study on Treatment of Industrial Wastewater by Catalytic Wet Oxidation*.

Nanjing University of Technology. Master's Thesis, 2006.

[29] L. Ren, W. Zhang, Present Situation and Future Development of Phenol-Containing Wastewater Treatment. Research Progress of Bioaugmentation Technology for Phenolic Wastewater, *Environmental Protection and Circular Economy*, Vol.34, No.7, 2014, pp. 46-48.

[30] D.L. Reyes, L. Raskin, Role of Filamentous Microorganisms in Activated Sludge Foamingrelationship of Mycolata Levels to Foaming Initiation and Stability, *Water*, Vol.36, No.2, 2002, pp. 445-459.

[31] P.R. Rodríguez, R.E. Palazon, A.M. Diez, S.H. Marsh, Delayed Coking: Industrial and Laboratory Aspects, *Carbon*, Vol.36, No.1-2, 1998, pp. 105-116.

[32] M.S. Shafiuddin, *Characterization of A Selected Refinery Wastewater Streams for Treatability Assessment*, Lamar University. Master's Thesis, 2016.

[33] S. Tabaatal, Y. Hamamoto, N. Hayakawa, K.S. Watanabe, *Activated Sludge Method*, Washington, DC: U.S. Patent and Trademark Office. U.S. Patent 4, 655, 925, 1987.

[34] B.Y. Wang, *Screening of Petroleum Degrading Bacteria and Its Application in Petrochemical Wastewater Treatment*, Northeast University. Master's Thesis, 2007.

[35] H.C. Wang, Innovation Direction of Activated Sludge Process in the Past Century, *Water & Wastewater Engineering*, Vol.10, 2014, pp. 1-3.

[36] N. Ghimire, S. Wang, *Biological Treatment of Petrochemical Wastewater, Petroleum Chemicals - Recent Insight*, From the Edited Volume, Edited by M. Zoveidavianpoor, IntechOpen, doi: 10.5772/intechopen.79655. 2018.

[37] M. Chugh, T. Chandak, S. Jha, D. Rawtani, Chapter 13: *Nanocellulose in Paper and Wood Industry*. In: R. Oraon, D. Rawtani, P. Singh, D.C.M. Hussain (eds), In Book: Nanocellulose Materials; Fabrication and Industrial Applications Micro and Nano Technologies, Elsevier, pp. 247–264, 2022.

[38] S. Cui, S. Zhang, S. Ge, L. Xiong, Q. Sun, Green Preparation and Characterization of Size-Controlled Nanocrystalline Cellulose via Ultrasonic-Assisted Enzymatic Hydrolysis, *Industrial Crops and Products*, Vol.83, 2016, pp. 346–352.

[39] K. Cura, N. Rintala, T. Kamppuri, E. Saarimäki, P. Heikkilä, Textile Recognition and Sorting for Recycling at an Automated Line Using Near Infrared Spectroscopy, *Recycling* Vol.6, No.1, 2021, 11, pp. 1–12.

[40] D. Damayanti, L.A. Wulandari, A. Bagaskoro, A. Rianjanu, H.-S. Wu, Possibility Routes for Textile Recycling Technology, *Polymers (Basel)*, Vol.13, No.21, 2021, 3834, pp. 1-31.

[41] J.H.O. do Nascimento, R.F. Luz, F.M.F. Galvão, J.D.D. Melo, F.R. Oliveira, R. Ladchumananandasivam, A. Zille, Extraction and Characterization of Cellulosic Nanowhisker Obtained from Discarded Cotton Fibers, *Materials Today Proceedings*, Vol.2, No.1, 2015, pp. 1–7.

[42] T.K.Q. Doan, K.Y. Chiang, Characteristics and Kinetics Study of Spherical Cellulose Nanocrystal Extracted from Cotton Cloth Waste by Acid Hydrolysis, *Sustainable Environment Research*, Vol.32, 2022, Article number:26, pp. 1-14.

[43] M.S. Mignon Dunbar, T.M. Murphy, DNA Analysis of Natural Fiber Rope, *Journal of Forensic Sciences*, Vol.54, No.1, 2009, pp. 108–113.

[44] M. El Achaby, Z. Kassab, A. Aboulkas, C. Gaillard, A. Barakat, Reuse of Red Algae Waste for the Production of Cellulose Nanocrystals and Its Application in Polymer Nanocomposites, *International Journal of Biological Macromolecules*, Vol.106, 2018, pp. 681–691.

[45] N. Eslahi, F. Dadashian, N.H. Nejad, Optimization of Enzymatic Hydrolysis of Wool Fbers for Nanoparticles Production Using Response Surface Methodology, *Advanced Powder Technology*, Vol.24, No.1, 2013, pp. 416–426.

[46] T. Eriksson, J. Börjesson, F. Tjerneld, Mechanism of Surfactant Effect in Enzymatic Hydrolysis of Lignocellulose. *Enzyme and Microbial Technology*, Vol.31, No.3, 2002, pp. 353–364.

[47] F.A. Esteve-Turrillas, M. de la Guardia, Environmental Impact of Recover Cotton in Textile Industry, *Resources, Conservation and Recycling*, Vol.116, 2017, pp. 107-115.

[48] European Circular Economy Stakeholder Platform (2019), *Siptex: A Pioneering Textile Sorting Technology for Increased Circularity*, https://circulareconomy.europa.eu/platform/en/good-practices/siptex-pioneering-textile-sorting-techn ology-increased-circularity., Accessed 11 March 2025.

[49] European Environment Agency (2024), *Management of Used and Waste Textiles in Europe's Circular Economy,* https://www.eea.europa.eu/publications/manag

ementof-used-and-waste-textiles, Accessed 11 March 2025.

[50] European Parliament (2024) *The Impact of Textile Production and Waste on the Environment (Infographics)*. https://www.europarl.europa.eu/topics/en/article/20201208ST O93327/the-impact-of-textile-production-and-wasteon-the-environment-infographics., Accessed 11 March 2025.

[51] R.R. Ferreira, A.G. Souza, L.L. Nunes, N. Shahi, V.K. Rangari, D. dos Santos Rosa, Use of Ball Mill to Prepare Nanocellulose from Eucalyptus Biomass: Challenges and Process Optimization by Combined Method, *Materials Today Communications*, Vol.22, 2020, 100755.

[52] F.V. Ferreira, A.G. Souza, R. Ajdary, L.P. de Souza, J.H. Lopes, D.S. Correa, G. Siqueira, H.S. Barud, D. dos S. Rosa, L.H.C. Mattoso, O.J. Rojas, Nanocellulose-based Porous Materials: Regulation and Pathway to Commercialization in Regenerative Medicine, *Bioactive Materials*, Vol.29, 2023, pp. 151-176.

[53] A. García, A. Gandini, J. Labidi, N. Belgacem, J. Bras, Industrial and Crop Wastes: A New Source for Nanocellulose Biorefnery, *Industrial Crops and Products*, Vol.93, 2016, pp. 26-38.

[54] J. Gong, J. Li, J. Xu, Z. Xiang, L. Mo, Research on Cellulose Nanocrystals Produced from Cellulose Sources with Various Polymorphs, *RSC Advances*, Vol.7, 2017, pp. 33486-33493.

[55] M. Gibril, T. Tesfaye, B. Sithole, P. Lekha, D. Ramjugernath, Optimisation and Enhancement of Crystalline Nanocellulose Production by Ultrasonic Pretreatment of Dissolving Wood Pulp Fibres, *Cellulose Chemistry and Technology*, Vol.52, No.9-10, 2018, pp. 711-727.

[56] A. Gil, Current Insights into Lignocellulose Related Waste Valorization, *Chemical Engineering Journal Advances*, Vol.8, 2021, 100186.

[57] S.H. Mohamed, Md. Sohrab Hossain, M.H.M. Kassim, M.I. Ahmad, F.M. Omar, V. Balakrishnan, M. Zulkifli, A.N. Ahmad Yahaya, Recycling Waste Cotton Cloths for the Isolation of Cellulose Nanocrystals: A Sustainable Approach, *Polymers (Basel)*, Vol.13, No.4, 2021, 626, pp. 1-17.

[58] M. Moniruzzaman, T. Ono, Separation and Characterization of Cellulose Fibers from Cypress Wood Treated with Ionic Liquid Prior to Laccase Treatment, *Bioresource Technology*, Vol.127, 2013, pp. 132-137.

[59] S. Mondal, Preparation, Properties and Applications of Nanocellulosic Materials, *Carbohydrate Polymers*, Vol.163, 2017, pp. 301-316.

[60] J.P.S. Morais, M. de Freitas Rosa, M.M. de Souza Filho, L.D. Nascimento, D.M. do Nascimento, A.R. Cassales, Extraction and Characterization of Nanocellulose Structures from Raw Cotton Linter, *Carbohydrate Polymers*, Vol.91, 2013, pp. 229-235.

[61] M. Nasir, R. Hashim, O. Sulaiman, M. Asim, *Nanocellulose: Preparation Methods and Applications*, In: M. Jawaid, S. Bouf, HPSAK (eds) Woodhead Publishing Series in Composites Science and Engineering, Cellulose Reinforced Nanofibre Composites, Woodhead Publishing, pp. 261-276, 2017.

[62] A. Naderi, T. Lindström, J. Sundström, Carboxymethylated Nanofibrillated Cellulose: Rheological Studies, *Cellulose,* Vol.21, 2014, pp. 1561-1571.

[63] K. Niinimäki, G. Peters, H. Dahlbo, P. Perry, T. Rissanen, A. Gwilt, The Environmental Price of Fast Fashion, *Nature Reviews Earth & Environment*, Vol.1, 2020, pp. 189-200.

[64] N. Pandi, S.H. Sonawane, K. Anand Kishore, Synthesis of Cellulose Nanocrystals (CNCs) from Cotton Using Ultrasound-Assisted Acid Hydrolysis, *Ultrasonics Sonochemistry*, Vol.70, 2021, 105353.

[65] A. Patti, G. Cicala, D. Acierno, Eco-Sustainability of the Textile Production: Waste Recovery and Current Recycling in the Composites World, *Polymers (Basel)*, Vol.13, 2021, pp. 1-22.

[66] P. Phanthong, G. Guan, Y. Ma, X. Hao, A. Abudula, Effect of Ball Milling on the Production of Nanocellulose Using Mild Acid Hydrolysis Method, *Journal of the Taiwan Institute of Chemical Engineers*, Vol.60, 2016, pp. 617-622.

[67] P. Phanthong, P. Reubroycharoen, X. Hao, G. Xu, A. Abudula, G. Guan, Nanocellulose: Extraction and Application, *Carbon Resources Conversion*, Vol.1, No.1, 2018, pp. 32-43.

[68] W.C. Lipps, E.B. Braun-Howland, T.E. Baxter, *Standard Methods for the Examination of Water and Wastewater*, 24th. Edition, W.C. Lipps, E.B. Braun-Howland, T.E. Baxter, (editors), American Public Health Association (APHA), American Water Works Association (AWWA), Water Environment Federation (WEF), Elevate Your Standards. American Public Health Association 800 I Street, NW Washington DC: 20001-3770, USA, December 1, 2022; ISBN:9780875532998.

[69] A. Poulose, J. Parameswaranpillai, J.J. George, J.A. Gopi, S. Krishnasamy, M. Dominic, N. Hameed, N.V. Salim, S. Radoor, N. Sienkiewicz, Nanocellulose: A Fundamental Material for Science and Technology Applications, *Molecules* Vol.27, No.22, 2022, 8032, pp. 1-27.

[70] D. Pradhan, A.K. Jaiswal, S. Jaiswal, Emerging Technologies for the Production of Nanocellulose from Lignocellulosic Biomass, *Carbohydrate Polymers*, Vol.285, 2022, 119258.

[71] S.S. Rahman, S. Siddiqua, C. Cherian, Sustainable Applications of Textile Waste Fiber in the Construction and Geotechnical Industries: A Retrospect, *Cleaner Engineering and Technology*, Vol.6, 2022, 100420.

[72] V. Raju, R. Revathiswaran, K.S. Subramanian, K.T. Parthiban, K. Chandrakumar, E.V. Anoop, C.J. Chirayil, Isolation and Characterization of Nanocellulose from Selected Hardwoods, viz., Eucalyptus tereticornis Sm. and Casuarina equisetifolia L., by Steam Explosion Method, *Scientific Reports*, Vol.13, 2023, Article number: 1199, pp. 1-15.

[73] A.K. Rana, E. Frollini, V.K. Thakur, Cellulose Nanocrystals: Pretreatments, Preparation Strategies, and Surface Functionalization, *International Journal of Biological Macromolecules*, Vol.182, 2021, pp. 1554-1581.

[74] M. Raza, B. Abu-Jdayil, F. Banat, A.H. Al-Marzouqi, Isolation and Characterization of Cellulose Nanocrystals from Date Palm Waste, *ACS Omega*, Vol.7, No.29, 2022, pp. 25366-25379.

[75] R.S.A. Ribeiro, B.C. Pohlmann, V. Calado, N. Bojorge, N. Pereira Jr., Production of Nanocellulose by Enzymatic Hydrolysis: Trends and Challenges, *Engineering in Life Sciences*, Vol.19, No.4, 2019, pp. 279-291.

[76] N. Rintala, NIRS Identification of Black Textiles: Improvements for Waste Textiles Sorting, Lahti University of Applied Sciences, Bachelor’s Thesis, 2019.

[77] V. Apostolopoulou-Kalkavoura, A.P. Mathew, Unlocking the Potential of Post-Consumer Garments as a Source of Nanocellulose, *Cell Reports Physical Science*, Vol.5, No.2, 2024, 101795.

[78] M.-X. Ruiz-Caldas, J. Carlsson, I. Sadiktsis, A. Jaworski, U. Nilsson, A.P. Mathew, Cellulose Nanocrystals from Postconsumer Cotton and Blended Fabrics: A Study on Their Properties, Chemical Composition, and Process Efficiency, *ACS Sustainable Chemistry & Engineering*, Vol.10, No.11, 2022, pp. 3787-3798.

[79] G. Sandin, G.M. Peters, Environmental Impact of Textile Reuse and Recycling: A Review, *Journal of Cleaner Production*, Vol.184, 2018, pp. 353-365.

[80] F.T. Seta, X. An, L. Liu, H. Zhang, J. Yang, W. Zhang, S. Nie, S. Yao, H. Cao, Q. Xu, Y. Bu, H. Liu, Preparation and Characterization of High Yield Cellulose Nanocrystals (CNC) Derived from Ball Mill Pretreatment and Maleic Acid Hydrolysis, *Carbohydrate Polymers*, Vol.234, 2020, 115942.

[81] C. Sharma, N.K. Bhardwaj, Bacterial Nanocellulose: Present Status, Biomedical Applications and Future Perspectives, *Materials Science & Engineering C, Materials for Biological Applications*, Vol.104, 2019, 109963.

[82] L. Shen, J. Jiang, J. Liu, F. Fu, H. Diao, X. Liu, Cotton Fabrics with Antibacterial and Antiviral Properties Produced by a Simple Pad-Dry-Cure Process Using Diphenolic Acid, *Applied Surface Science*, Vol.600, 2022, 154152.

[83] W. Shuhua, Y. Xiaoying, C. Xiaogang, H. Wensheng, N. Mei, Recycling of Cotton Fibers Separated from the Waste Blend Fabric, *Journal of Natural Fibers*, Vol.17, 2020, pp. 520-531.

[84] C.R. Soccol, V. Faraco, S. Karp, L.P.S. Vandenberghe, V. Thomaz-Soccol, A. Woiciechowski, A. Pandey, Chapter 5: *Lignocellulosic Bioethanol: Current Status and Future Perspectives*. In: A. Pandey, C. Larroche, S.C. Ricke, E. Gnansounou, C.-G. Dussap (eds), In Book: Biofuels: Alternative Feedstocks and Conversion Processes, pp. 101-122, 2011.

[85] K. Song, Y. Ji, L. Wang, Y. Wei, Z. Yu, A Green and Environmental Benign Method to Extract Cellulose Nanocrystal by Ball Mill Assisted Solid Acid Hydrolysis, *Journal of Cleaner Production*, Vol.196, 2018, pp. 1169-1175.

[86] P. Srichola, K. Witthayolankowit, P. Sukyai, C. Sampoompuang, K. Lobyam, P. Kampakun, R. Toomtong, Recycling of Nanocellulose from Polyester-Cotton Textile Waste for Modifcation of Film Composites, *Polymers (Basel)*, Vol.15, No.15, 2023, 3324.

[87] Y.Y. Sun, Z.P. Xia, A.P. Yang, J.X. Li, L. Wang, H. Chen, X. Zheng, Y. Liu, Nanocellulose Extracted from Waste Polyester/Cotton Fabric by Chemical-Mechanical Separation Technology, *Journal of Physics: Conference Series*, Vol.1790, 2021, 012074.

[88] C. Tan, H. Chen, Z. Lin, T. Wu, Category İdentifcation of Textile Fibers Based on Near-Infrared Spectroscopy Combined with Data Description Algorithms, *Vibrational Spectroscopy*, Vol.100, 2019, pp. 71-78.

[89] A.H. Tayeb, E. Amini, S. Ghasemi, M. Tajvidi, Cellulose Nanomaterials-Binding Properties and Applications: A Review, *Molecules*, Vol.23, 2018, pp. 1-24.

[90] M.A. Teixeira, M.C. Paiva, M.T.P. Amorim, H.P. Felgueiras, Electrospun Nanocomposites Containing Cellulose and Its Derivatives Modifed with Specialized Biomolecules for an Enhanced Wound Healing, *Nanomaterials*, Vol.10, No.3, 2020, 557, pp. 1-64.

[91] H.L. Teo, R.A. Wahab, Towards an Eco-Friendly Deconstruction of Agro-Industrial Biomass and Preparation of Renewable Cellulose Nanomaterials: A Review, *International Journal of Biological macromolecules*, Vol.161, 2020, pp. 1414-1430.

[92] S. Thambiraj, D. Ravi Shankaran, Preparation and Physicochemical Characterization of Cellulose Nanocrystals from Industrial Waste Cotton, *Applied Surface Science*, Vol.412, 2017, pp. 405-416.

[93] D. Trache, A.F. Tarchoun, M. Derradji, T.S. Hamidon, N. Masruchin, N. Brosse, M.H. Hussin, Nanocellulose: From Fundamentals to Advanced Applications, *Frontiers in Chemistry*, Vol.8, 2020, Article: 392, pp. 1-33.

[94] A.B. Vanzetto, L.V.R. Beltrami, A.J. Zattera, Textile Waste as Precursors in Nanocrystalline Cellulose Synthesis, *Cellulose,* Vol.28, 2021, pp. 6967-6981.

[95] S. Ventura-Cruz, N. Flores-Alamo, A. Tecante, Preparation of Microcrystalline Cellulose from Residual Rose Stems (Rosa Spp.) by Successive Delignifcation with Alkaline Hydrogen Peroxide, *International Journal of Biological Macromolecules*, Vol.155, 2020, pp. 324-329.

[96] S. Ventura-Cruz, A. Tecante, Nanocellulose and Microcrystalline Cellulose from Agricultural Waste: Review on Isolation and Application as Reinforcement in Polymeric Matrices, *Food Hydrocolloids*, Vol. 118, 2021, 106771.

[97] B. Peng, Z. Yao, X. Wang, M. Crombeen, D.G. Sweeney, K.C. Tam, Cellulose-based Materials in Wastewater Treatment of Petroleum Industry, *Green Energy & Environment*, Vol.5, No.1, 2020, pp. 37-49.

[98] F. Aloulou, S. Boufia, J. Labidi, Modified Cellulose Fibres for Adsorption of Organic Compound in Aqueous Solution, *Separation and Purification Technology*, Vol.52, 2006, pp. 332-342.

[99] C. Li, X. Liu, K. Lv, J. Sun, C. Dai, B. Liao, C. Liu, C. Mei, Q. Wu, M. Hubbe, Cellulose Nanomaterials in Oil and Gas Industry: Current Status and Future Perspectives Mei, *Progress in Materials Science*, Vol.139, 2023, 101187.

[100] Q.A. Bader, Z.T. Al-Sharify, J.M. Dhabab, H.K. Zaidan, A.M. Rheima, D.M. Athair, T.M. Joseph, E. Kianfar, Cellulose Nanomaterials in Oil and Gas Industry and Bio-Manufacture: Current Situation and Future Outlook, *Case Studies in Chemical and Environmental Engineering*, Vol.10, 2024, 100993, pp.1-29.

[101] M.K. Jeddi, O. Laitinen, H. Liimatainen, Magnetic Superabsorbents Based on Nanocellulose Aerobeads for Selective Removal of Oils and Organic Solvents, *Materials & Design*, Vol.183, 2019, 108115, pp.1-10.

[102] L. Hao, Q. Zheng, Q. Zhuang, M. Guan, Z. Yin, J. Zeng, H. Chen, W. Wu, H. Zhou, X. Zhou, Antibacterial Microfibrillated Cellulose as Stimuli-Responsive Carriers with Enhanced UV Stability for Sustained Release of Essential Oils and Pesticides, *ACS Sustainable Chemistry and Engineering*, Vol.12, No.17, 2024, pp. 6666-6681.

[103] P. Stenstad, M. Andresen, B.S. Tanem, P. Stenius, Chemical Surface Modifications of Microfibrillated Cellulose, *Cellulose*, Vol.15, 2008, pp. 35-45.

[104] M. Madhushree, P. Vairavel, G.T. Mahesha, K. Subrahmanya Bhat, Oxidative Modifications of Cellulose: Methods, Mechanisms, and Emerging Applications, *Journal of Natural Fibers*, Vol.22, No.1, 2025, Article: 2497910, pp. 1-22.

Contribution of Individual Authors to the Creation of a Scientific Article (Ghostwriting Policy)

Prof. Dr. Delia Teresa Sponza and Post-Dr. Rukiye Öztekin took an active role in every stage of the preparation of this article.

The authors equally contributed in the present research, at all stages from the formulation of the problem to the final findings and solution.

Sources of Funding for Research Presented in a Scientific Article or Scientific Article Itself

The experimental phases of this research study were conducted at the National Research Council (NRC) of Canada, Research Centres, Ontario, Canada. The authors would like to thank this body for providing financial support.

Conflict of Interest

The authors have no conflicts of interest to declare that are relevant to the content of this article.

APPENDIX

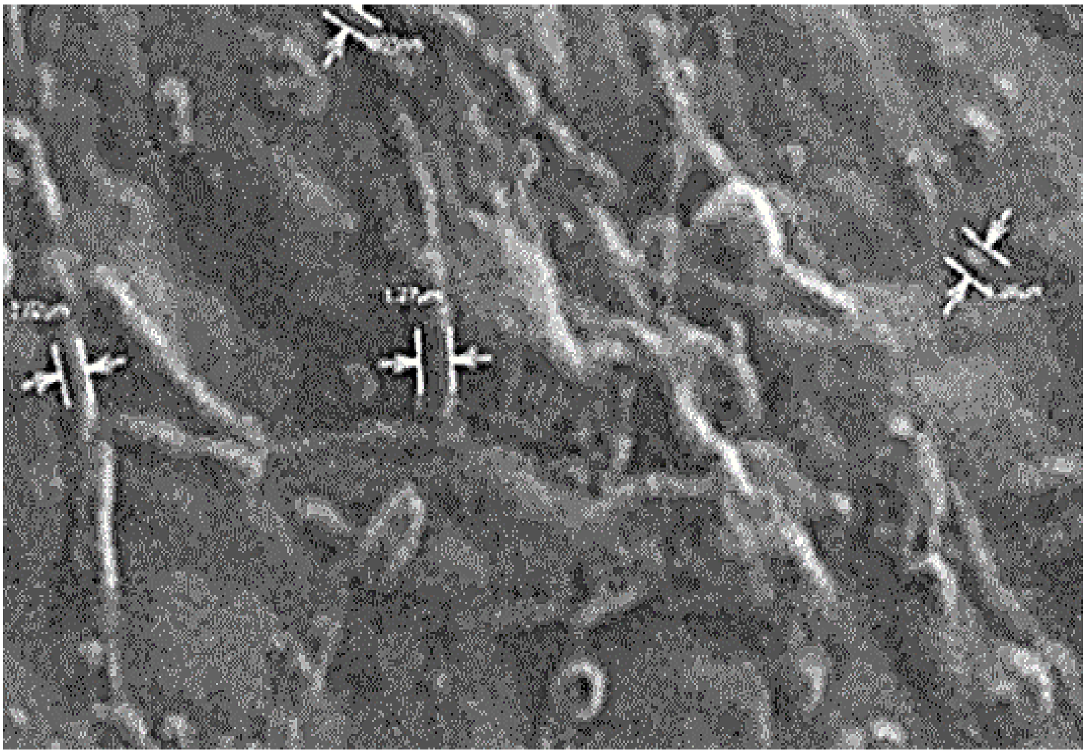

(a)

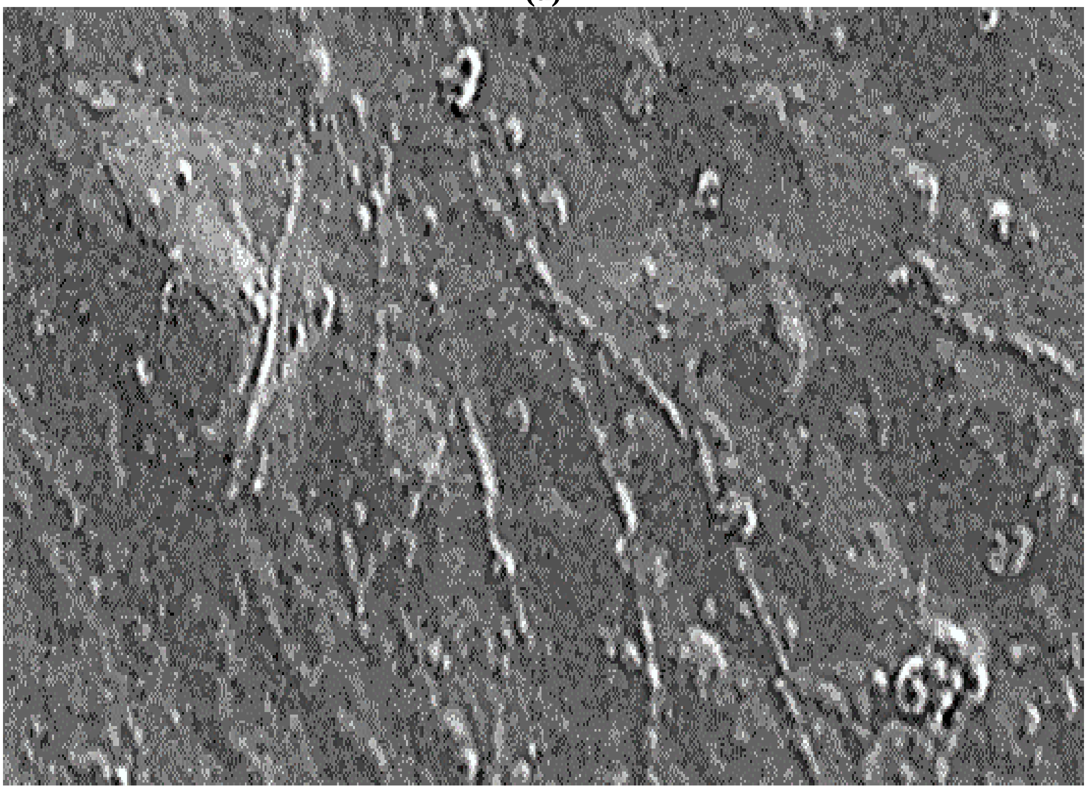

(b)

Fig. 1. SEM images of CNC **(a)** and CNC polymer structure **(b).**

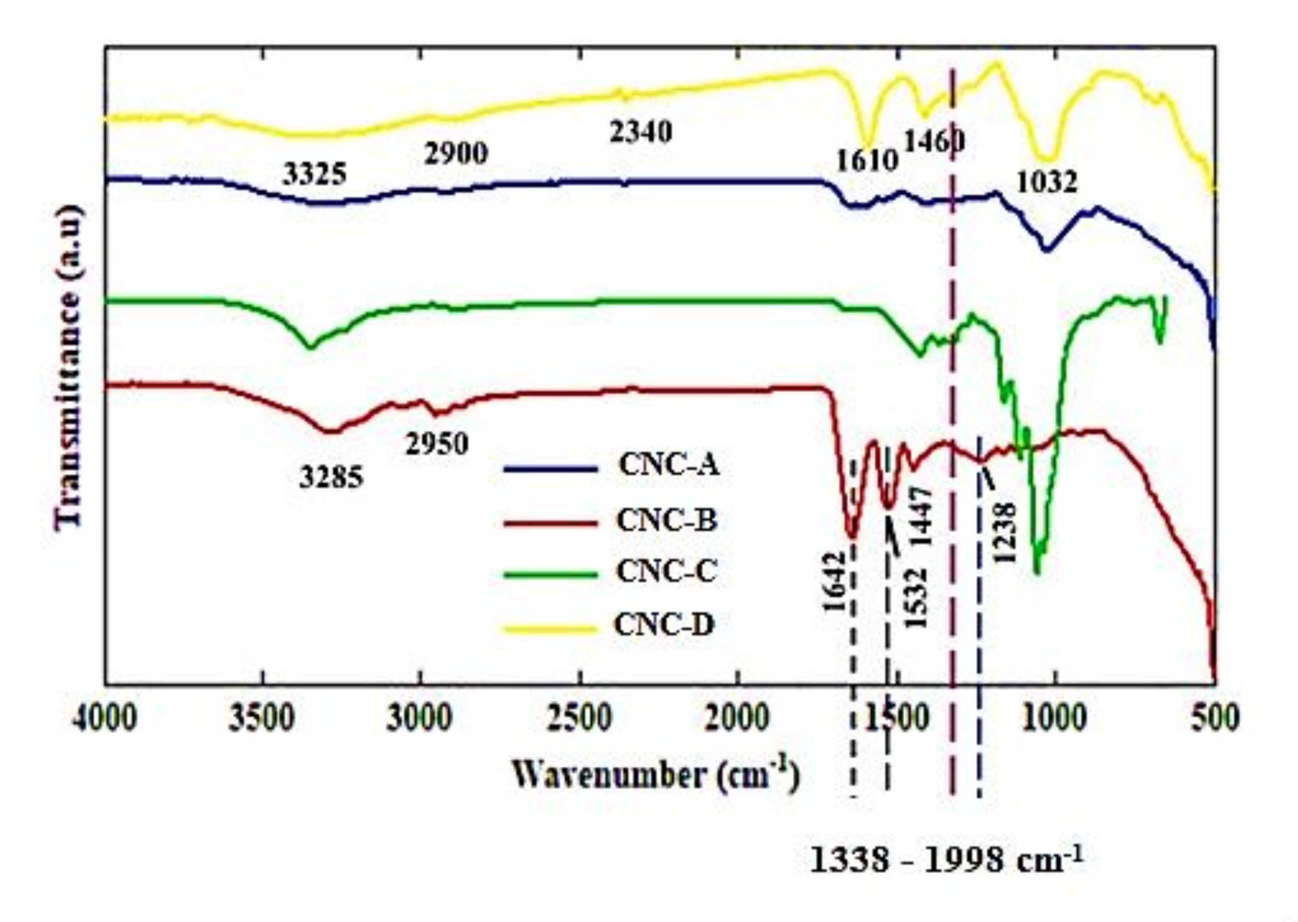

Fig. 2. FTIR spectra of prepared four CNC nanocomposites.

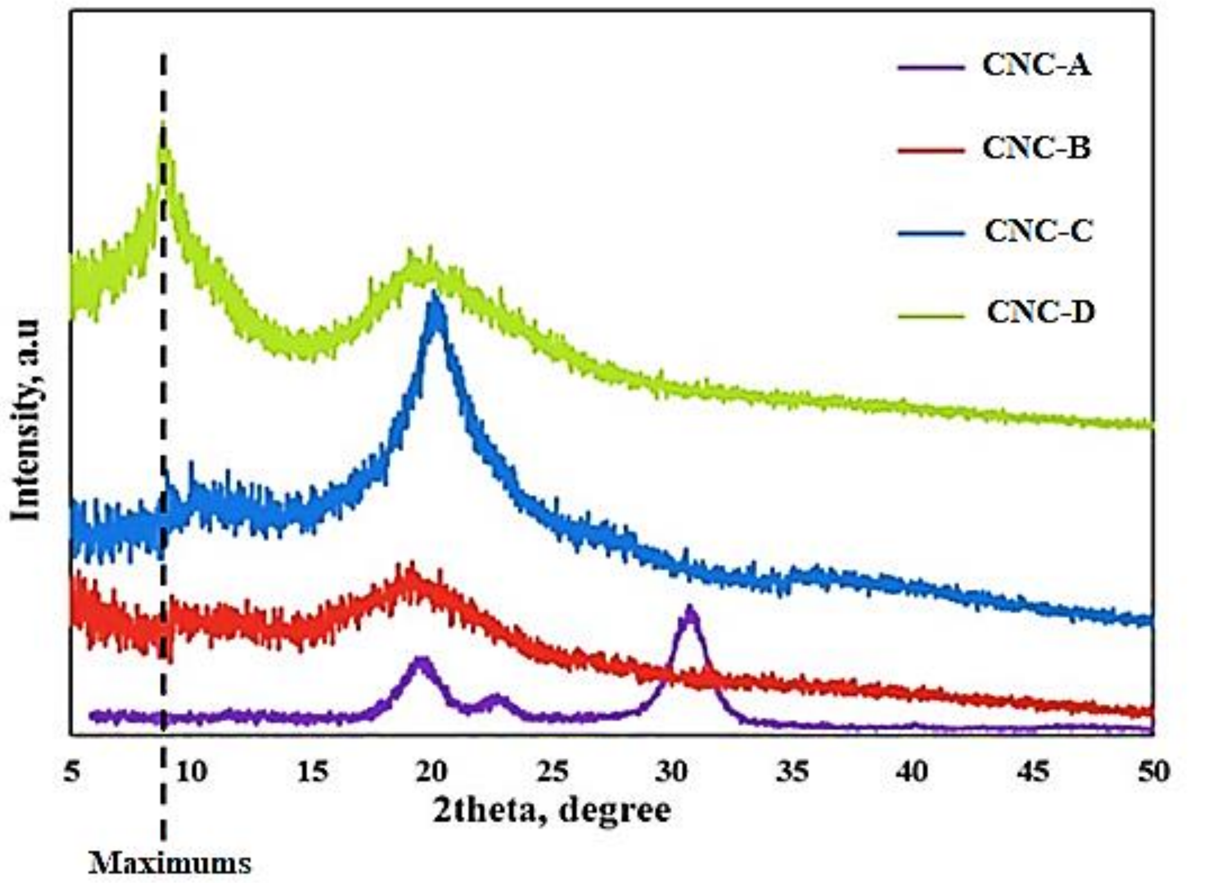

Fig. 3. XRD patterns of the four prepared CNC nanocomposites.

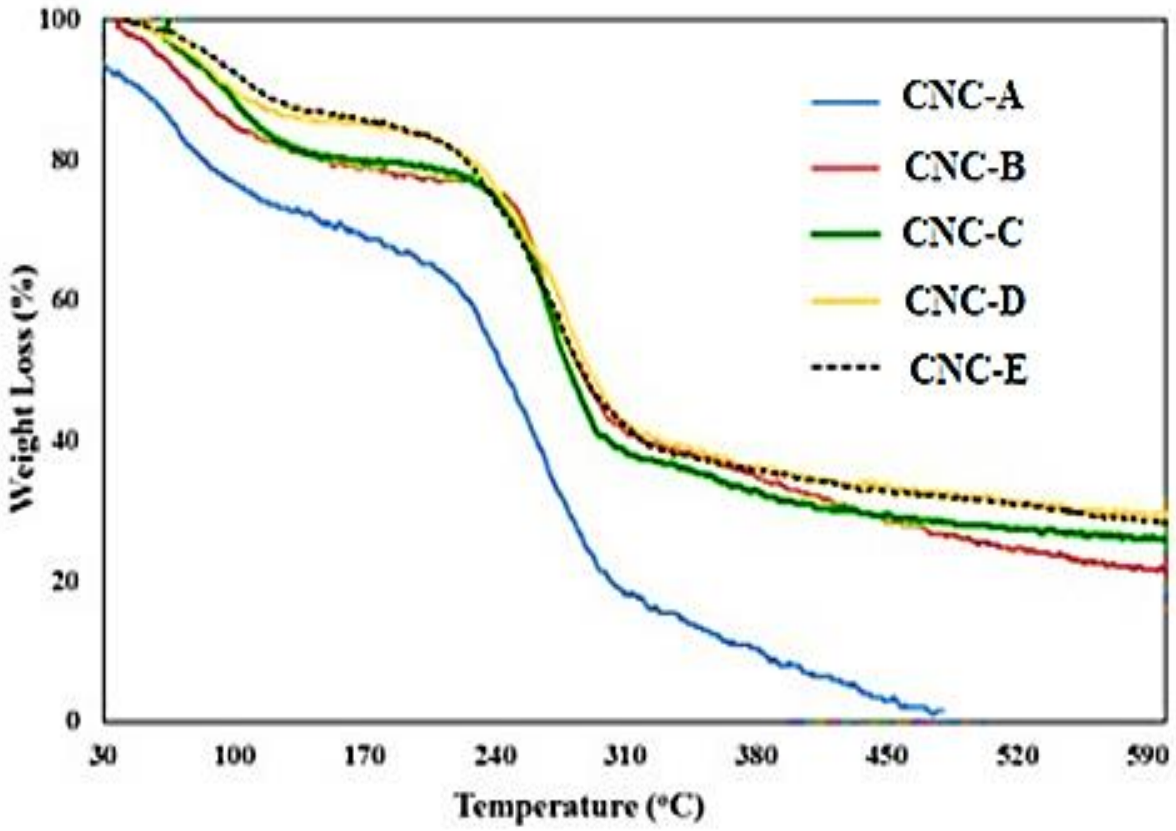

Fig. 4. TGA thermograms of five CNC nanocomposites.

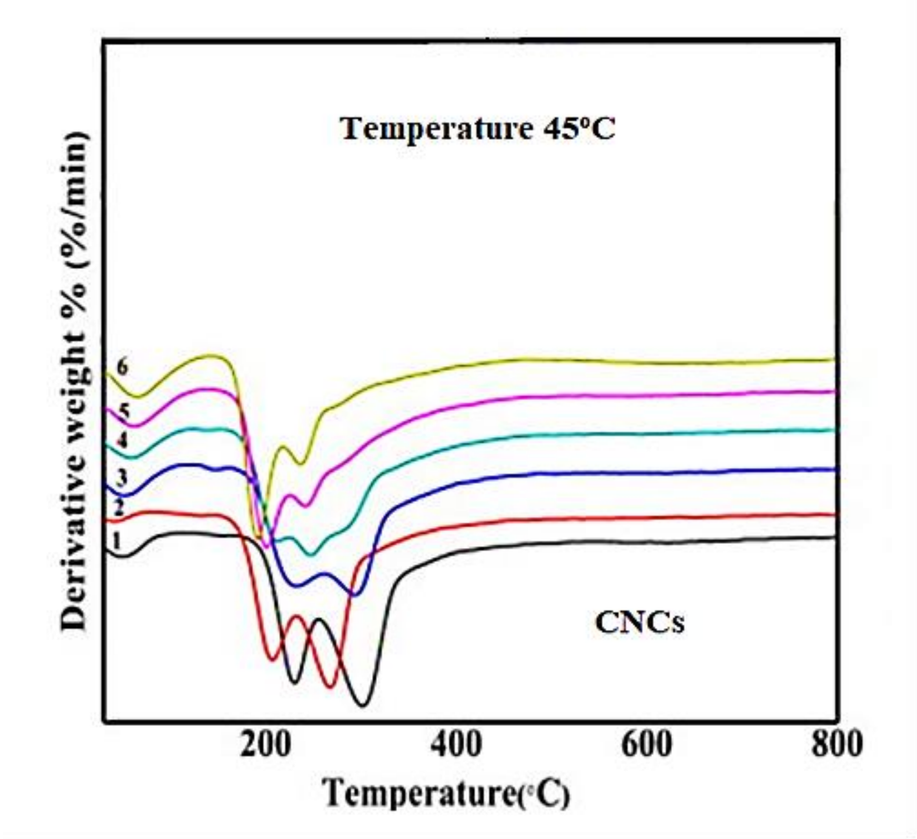

(a)

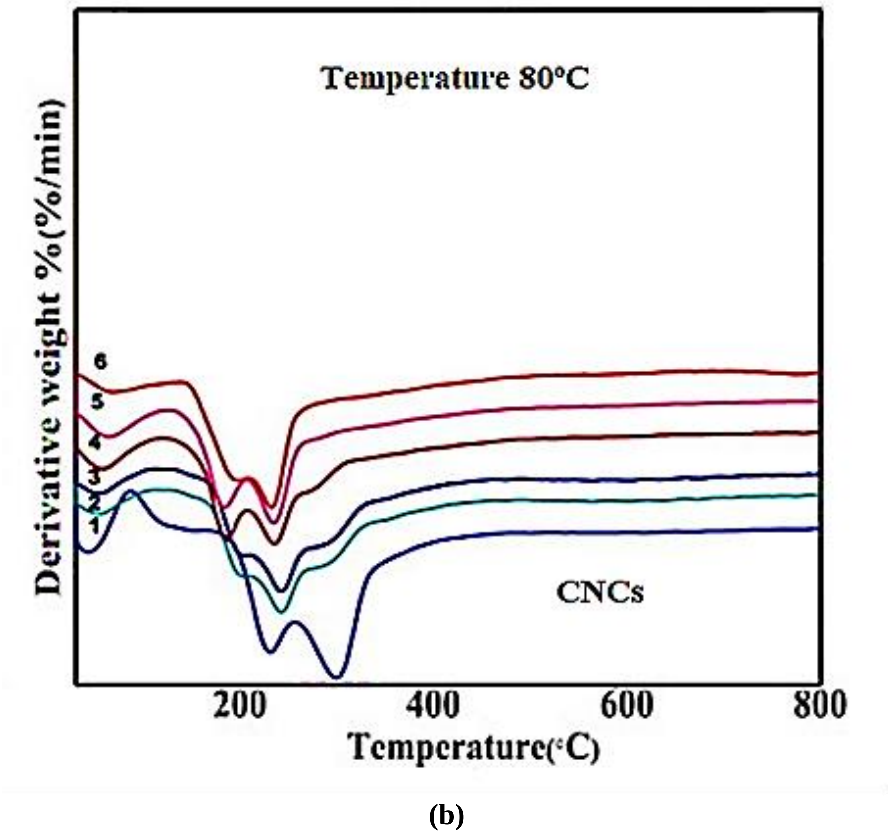

(b)

Fig. 5. DTG curves of six CNCs at increasing temperatures [CNC-A (1), CNC-B (2), CNC-C (3), CNC-D (4), CNC-E (5) and CNC-F (6)] **(a)** at 45^{o}C, **(b)** at 80^{o}C, **(c)** at 100^{o}C and **(d)** 120^{o}C, respectively.

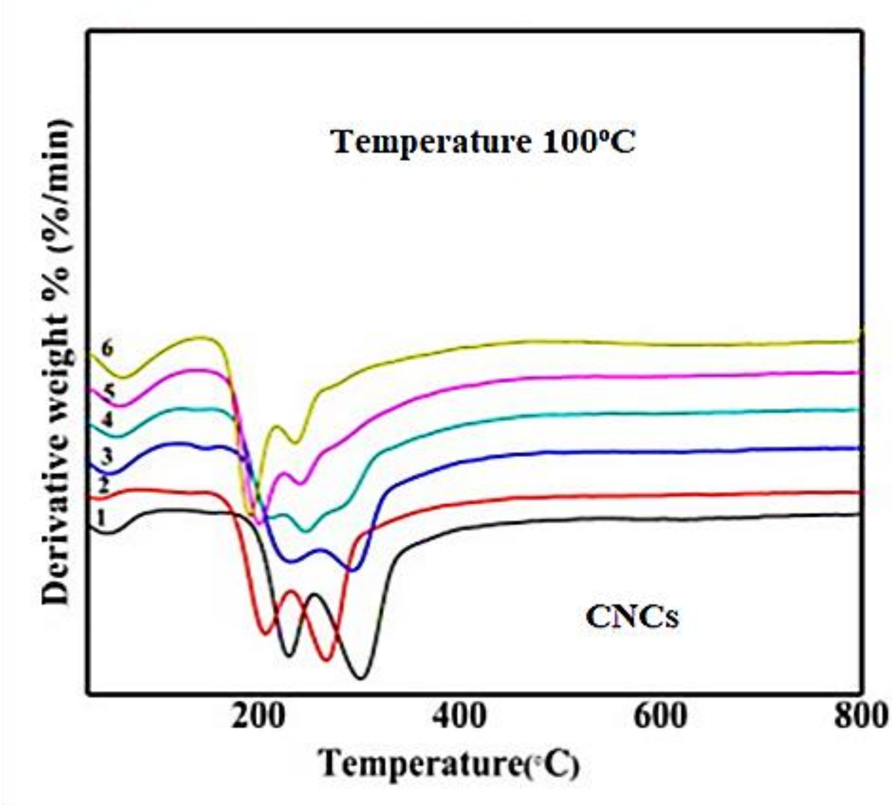

(c)

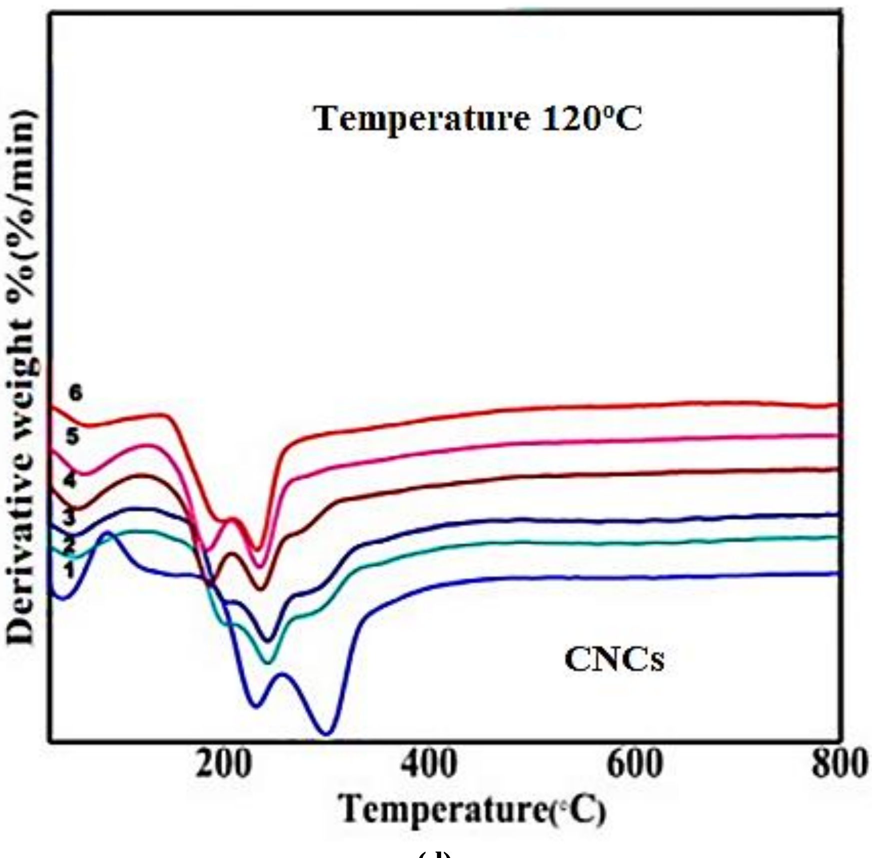

(d)

Fig. 5. (Cont.). DTG curves of six CNCs at increasing temperatures [CNC-A (1), CNC-B (2), CNC-C (3), CNC-D (4), CNC-E (5) and CNC-F (6)] **(a)** at 45ºC, **(b)** at 80ºC, **(c)** at 100ºC and **(d)** 120ºC, respectively.

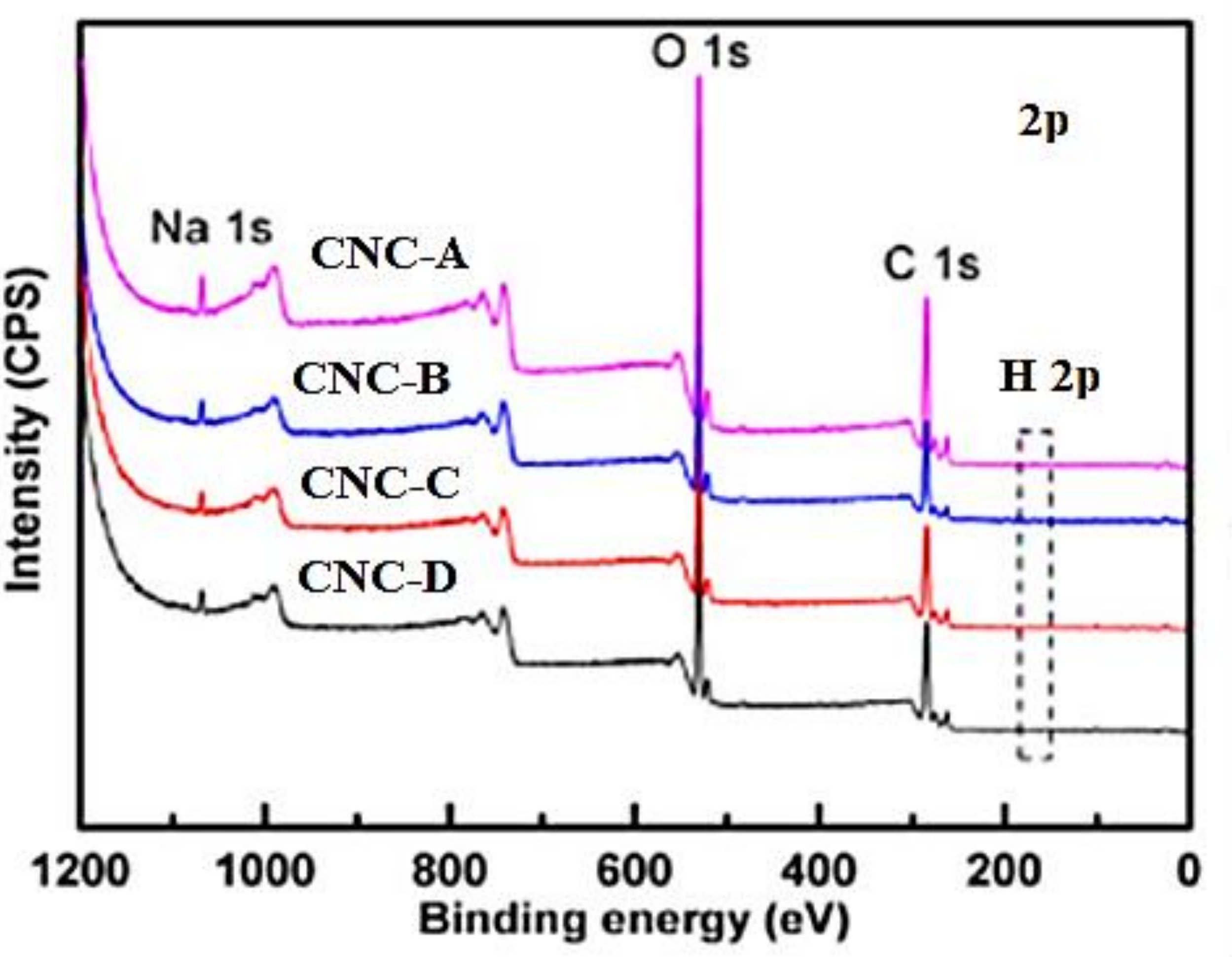

Fig. 6. XPS analysis of four types CNCs

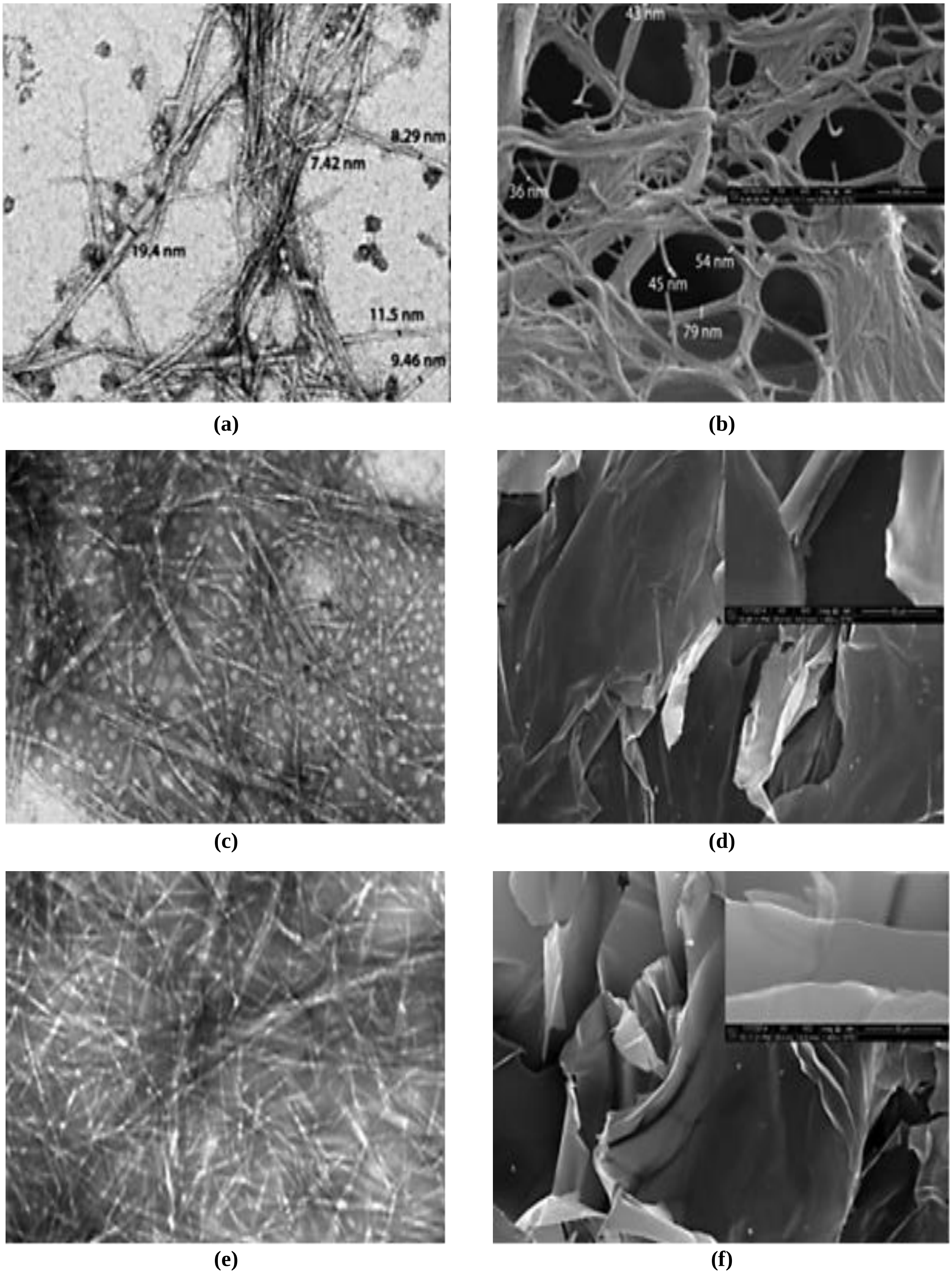

Fig. 7. TEM micrographs of CNC-A **(a)**, CNC-B **(b)**, CNC-C **(c)**, CNC-D **(d)**, CNC-E **(e)** and CNC-F **(f)**, respectively.

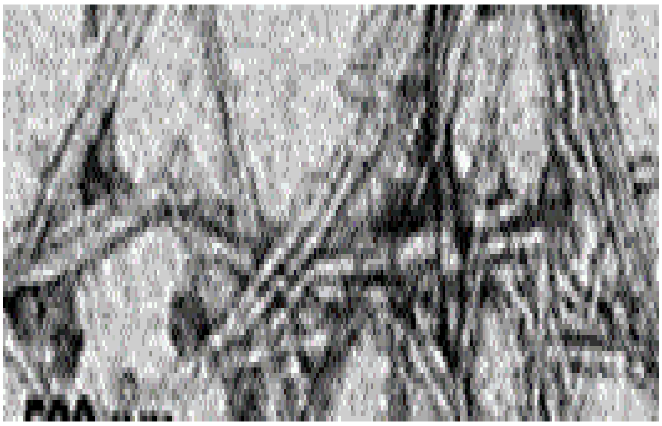

(a)

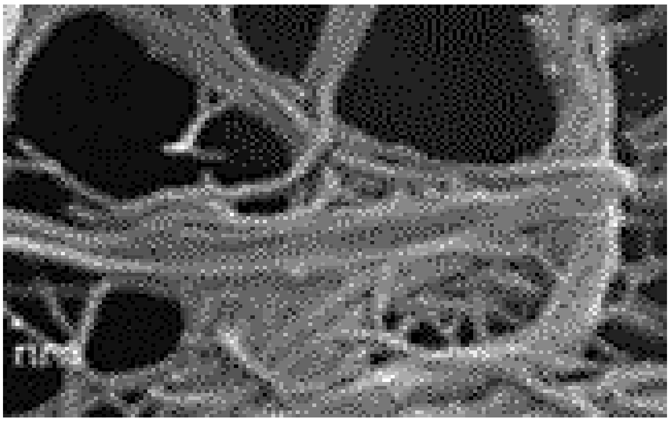

(b)

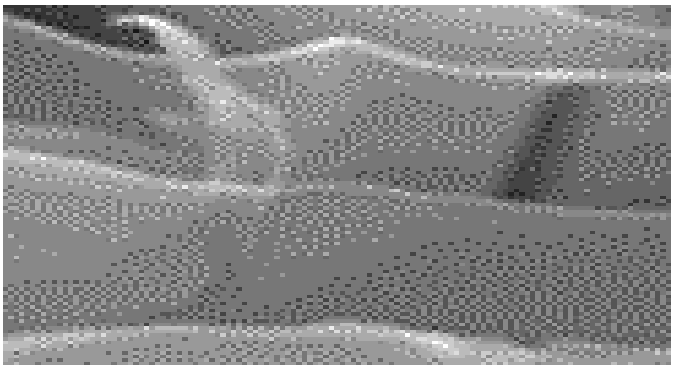

(c)

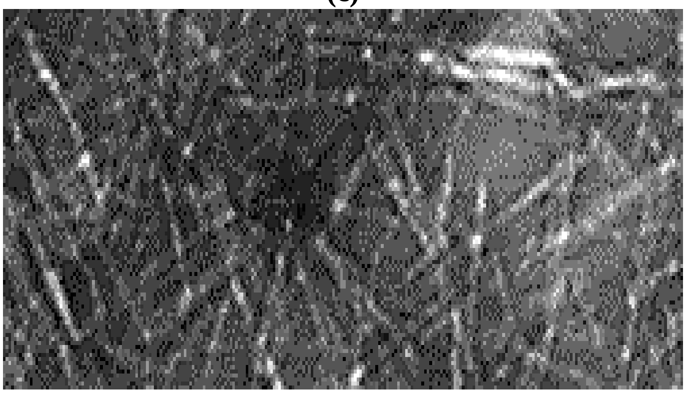

(d)

Fig. 8. FE-SEM analysis results of CNC-A **(a)**, CNC-B **(b)**, CNC-C **(c)** and CNC-D **(d)**, respectively.

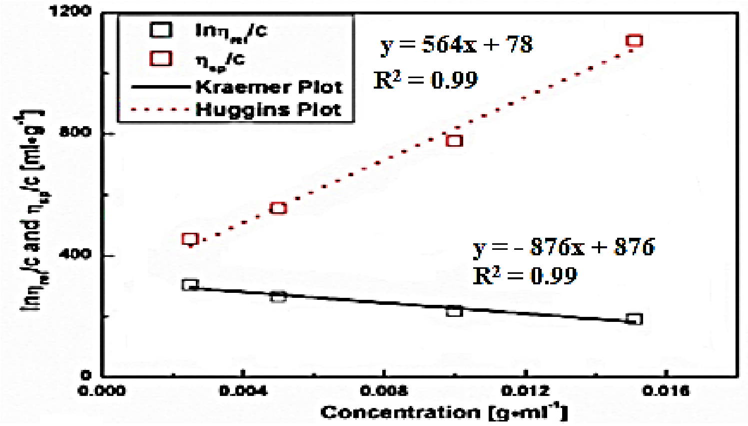

(a)

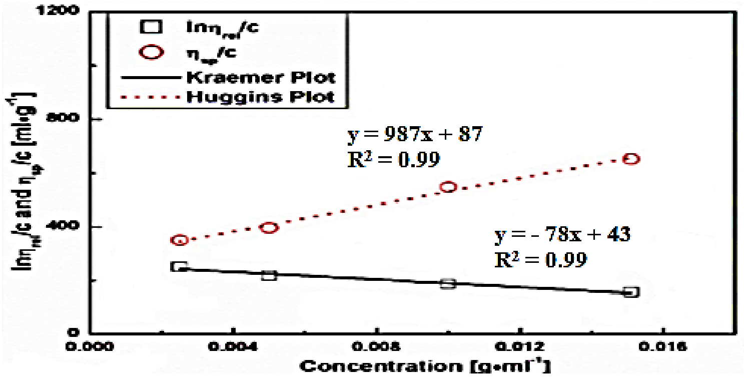

(b)

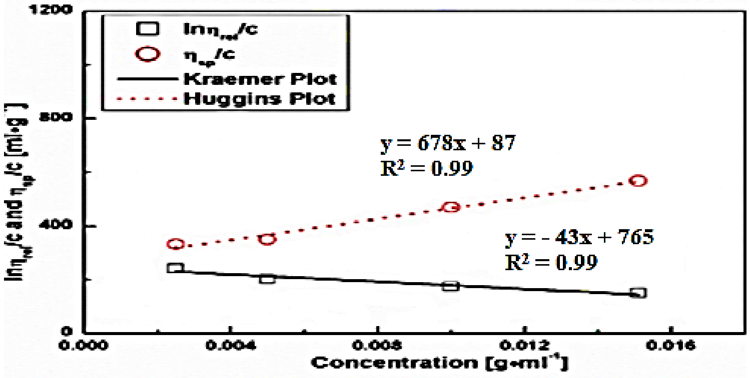

(c)

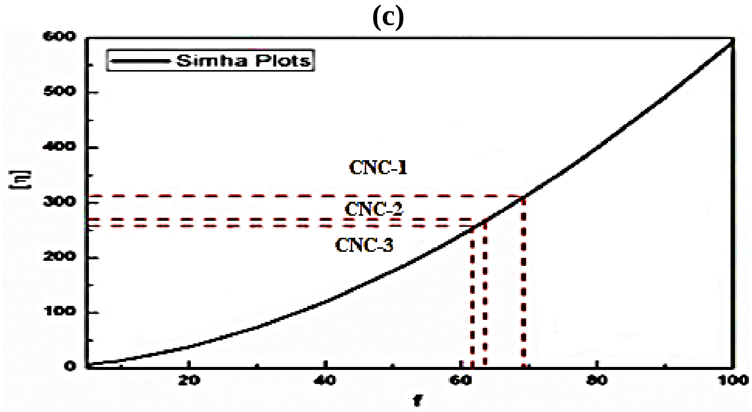

(d)

Fig. 9. Calculation of η and *f* values in CNC-1 **(a),** CNC-2 **(b),** CNC-3 **(c)** and CNC-1, CNC-2, CNC-3 **(d).**

Table 1. The maximum removal efficiencies of pollutant parameters (oil, DOC, DSS, toluene and m-xylene) in PCI ww with photoremoval process under optimum experimental conditions.

			Maximum Pollutants Removal Efficiencies (%)				
Parameters	**Optimum Experimental Conditions**	**Maximum Removal Yields (%)**	**Oil**	**DOC**	**DSS**	**Toluene**	**m-xylene**
Photoremoval Time (min)	after 150 min photoremoval time, at 25°C	99.60	84.11	96.71	98.40	91.20	93.40
pH Value	at pH=7.0, after 150 min photoremoval time, and at 25°C	99.20	89.40	98.22	98.83	92.35	94.39
Pollutant Concentrations (oil, DOC, DSS, toluene and m-xylene) (mg/l)	at 1000 mg/l pollutants concentrations, after 150 min photoremoval time, at pH=7.0, and at 25°C	99.48	91.70	99.13	99.47	93.50	96.21
CNCs Nanocomposites Concentrations (mg/l)	at 100 mg/l CNC nanocomposites concentrations, after 150 min photoremoval time, at pH=7.0, at 1000 mg/l pollutants concentrations, and at 25°C	99.76	99.30	99.10	99.52	95.64	99.05